Author Manuscript

Title: Structural and Mechanistic Insights into Development of Chemical Tools to Control Individual and Inter-related Pathological Features in Alzheimer's Disease

Authors: Hyuck Jin Lee; Kyle Korshavn; Younwoo Nam; Juhye Kang; Thomas Paul; Richard Kerr; Il Seung Yoon; Mehmet Ozbil; Kwang S. Kim; Brandon Ruotolo; Rajeev Prabhakar; Ayyalusamy Ramamoorthy; Mi Hee Lim

Structural and Mechanistic Insights into Development of Chemical Tools to Control Individual and Inter-related Pathological Features in Alzheimer's Disease

Hyuck Jin Lee,[a] Kyle J. Korshavn,[b] Younwoo Nam,[c] Juhye Kang,[c] Thomas J. Paul,[d] Richard A. Kerr,[b] Il Seung Youn,[c] Mehmet Ozbil,[d] Kwang S. Kim,[c] Brandon T. Ruotolo,[b] Rajeev Prabhakar,*[d] Ayyalusamy Ramamoorthy*[b,e] and Mi Hee Lim*[c]

Abstract: To elucidate the involvement of individual and inter-related pathological factors [*i.e.*, amyloid-β (Aβ), metals, and oxidative stress] in the pathogenesis of Alzheimer's disease (AD), chemical tools have been developed. Characteristics required for such tool construction, however, have not been clearly identified; thus, the optimization of available tools or new design has been limited. Herein, we report key structural properties and mechanisms that can determine tools' regulatory reactivities with multiple pathogenic features found in AD. We built up a series of small molecules *via* rational structural selection and variations [(i) location and number of an Aβ interacting moiety; (ii) metal binding site; (iii) denticity and structural flexibility] onto the framework of a tool useful for *in vitro* and *in vivo* metal–Aβ investigation. Detailed biochemical, biophysical, and computational studies using our chemical series were able to provide a foundation of how to originate molecular formulas to devise chemical tools capable of controlling the reactivities of various pathological components through distinct mechanisms. Overall, our multidisciplinary investigations illustrate a structure-mechanism-based strategy of tool invention for such a complicated brain disease, AD.

Introduction

Alzheimer's disease (AD) is a progressive and fatal brain disorder that is defined by progressive neuronal loss and cognitive defects.[1] Due to the unclear and complicate etiology of AD, a cure for the disease has not been discovered. Amyloid-β (Aβ) peptides are suggested to be associated with AD pathogenesis since misfolded Aβ aggregates are primary components of senile plaques found in the AD-afflicted brain (amyloid cascade hypothesis).[1,2] Upon the proteolytic cleavage of amyloid precursor protein (APP) by β- and γ-secretases, Aβ peptides are produced [two major isoforms, $A\beta_{40}$ and $A\beta_{42}$ (*ca.* 90% and 9% in the brain, respectively), which are aggregation-prone to form aggregates from various-sized oligomers to mature fibrils].[1a-c,2] Based on recent findings, soluble Aβ oligomers are observed to be toxic; however, a relationship between Aβ conformations and toxicity remains uncertain.[1c,2] Moreover, the AD-affected brain exhibits highly concentrated metal ions within senile plaques [*e.g.*, *ca.* 0.4 mM for $Cu^{I/II}$, 1.0 mM for Zn^{II}, 0.9 mM for $Fe^{II/III}$].[1d,3] Previous *in vitro* studies present that these metal ions [particularly, $Cu^{I/II}$ and Zn^{II}] can interact with Aβ peptides and facilitate peptide aggregation. Furthermore, complexes of Aβ and redox-active metal ions, such as $Cu^{I/II}$ and $Fe^{II/III}$, are shown to overproduce reactive oxygen species (ROS) *via* Fenton-like reactions leading to oxidative stress.[1b-d,3] Thus, it has been proposed that individual or inter-related reactivities of metal-free Aβ, metal ions, and ROS may contribute to AD pathogenesis [specially, *via* an inter-communicator, metal-bound Aβ (metal–Aβ)] (Figure 1).[1c,1d,3d,3e]

To elucidate the molecular-level underpinnings of individual and inter-related risk features involved in AD pathogenesis, small molecules capable of targeting and modulating their reactivities have been developed as chemical tools.[4] Among them, **L2-b** (N^1,N^1-dimethyl-N^4-(pyridin-2-ylmethyl)benzene-1,4-diamine; Figure 1) was recently developed for regulating metal–Aβ species, along with antioxidant activity, and its *in vitro* and *in vivo* efficacy toward metal–Aβ was demonstrated.[4b,4f] Until now, however, it has not been determined which and how the molecular formulas and properties of such the tool could lead to its reactivities specific for the desired target, which has restricted new or innovative tool development. Herein, we report our multidisciplinary studies employing a chemical library newly designed based on **L2-b**'s backbone (Figure 1) that demonstrate the importance of rationally constructing and tuning structural features and mechanisms (*e.g.*, peptide modifications, including degradation and covalent adduct formation, *via* oxidative transformations of small molecules based on their ionization potentials) toward development of tools for regulating distinct

[a] Dr. Hyuck Jin Lee
School of Life Sciences
Ulsan National Institute of Science and Technology (UNIST)
Ulsan 44919 (Republic of Korea)

[b] Dr. Kyle J. Korshavn, Dr. Richard A. Kerr, Prof. Dr. Brandon T. Ruotolo, Prof. Dr. Ayyalusamy Ramamoorthy
Department of Chemistry, University of Michigan
Ann Arbor, Michigan 48109 (USA)
E-mail: ramamoor@umich.edu (A. Ramamoorthy)

[c] Younwoo Nam, Dr. Il Seung Youn, Juhye Kang, Prof. Dr. Kwang S. Kim and Prof. Dr. Mi Hee Lim
Department of Chemistry, UNIST
E-mail: mhlim@unist.ac.kr (M. H. Lim)

[d] Thomas J. Paul, Dr. Mehmet Ozbil, Prof. Dr. Rajeev Prabhakar
Department of Chemistry
University of Miami
Coral Gables, Florida 33146 (USA)
E-mail: rpr@miami.edu (R. Prabhakar)

[e] Prof. Dr. Ayyalusamy Ramamoorthy
Biophysics, University of Michigan

Supporting information for this article is given *via* a link at the end of the document.
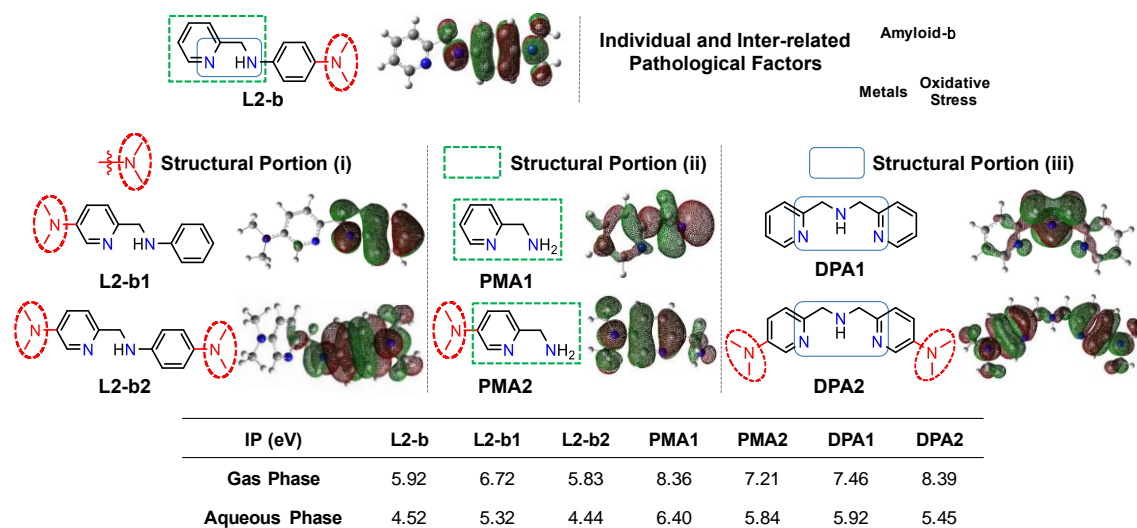
Figure 1. Structural investigations (i-iii) of small molecules to alter their ionization potentials (IPs) and reactivities with individual and inter-related AD pathological factors. Structural variations: (i) the different position and number of the dimethylamino functionality; (ii) the metal binding sites with and without a dimethylamino group; (iii) the increased denticity and structural flexibility. Potential donor atoms for metal binding are indicated in blue. Isosurface plots of compounds' SOMOs (blue, N; gray, C; white, H) are depicted underneath of compounds' structures. The calculated IPs in both the gas and aqueous phases are summarized in the table (bottom). **L2-b**, N^1,N^1-dimethyl-N^4-(pyridin-2-ylmethyl)benzene-1,4-diamine; **L2-b1**, N,N-dimethyl-6-((phenylamino)methyl)pyridin-3-amine; **L2-b2**, N^1-((5-(dimethylamino)pyridin-2-yl)methyl)-N^4,N^4-dimethylbenzene-1,4-diamine; **PMA1**, pyridin-2-yl-methanamine; **PMA2**, 6-(aminomethyl)-N,N-dimethylpyridin-3-amine; **DPA1**, bis(pyridin-2-ylmethyl)amine; **DPA2**, 6-((((5-(dimethyl-amino)pyridin-2-yl)methyl)amino)methyl)-N,N-dimethylpyridin-3-amine.

IP (eV)	L2-b	L2-b1	L2-b2	PMA1	PMA2	DPA1	DPA2
Gas Phase	5.92	6.72	5.83	8.36	7.21	7.46	8.39
Aqueous Phase	4.52	5.32	4.44	6.40	5.84	5.92	5.45

and inter-related pathological features in AD. Moreover, through the design principle gained from structural and mechanistic details, a chemical tool for targeting and controlling multiple distinguishable factors (*i.e.*, metals, metal-free Aβ, metal–Aβ, and oxidative stress) was successfully constructed. Overall, our studies illustrate an instruction of how chemical tools can be devised for investigating individual or inter-related pathological factors in AD.

Results and Discussion

Rational selection and preparation of small molecules

In order to establish how structural characteristics can guide mechanistic directions of chemical tools for desired reactivities toward their distinct targets, a class of small molecules derived from the backbone of **L2-b** was rationally designed (Figure 1). In our chemical series, different structural variations or portions

based on the framework of **L2-b** were applied or selected (Figure 1): (i) the position and number of the dimethylamino functionality, important for Aβ interaction,[4a-g,5] on the backbone of **L2-b** were altered affording **L2-b1** and **L2-b2**; (ii) the structural moieties of **L2-b** and **L2-b1**/**L2-b2** for metal binding (*i.e.*, **PMA1** and **PMA2**, respectively) were included; (iii) the denticity and structural flexibility on **L2-b**'s structure were varied generating **DPA1** and **DPA2**. Moreover, the blood-brain barrier (BBB) permeability of our compounds was also considered for their biological applications. The potential BBB penetration of small molecules was suggested based on Lipinski's rules as well as the values obtained from logBB calculation and the Parallel Artificial Membrane Permeability Assay adapted for the BBB (PAMPA-BBB)[4b,4c,4d,6] (Supporting Information, Table S1).

L2-b, **L2-b1**, **L2-b2**, and **DPA2** were prepared following the previously reported methods with slight modifications (especially for **L2-b1**, **L2-b2**, and **DPA2**, the procedures are summarized Scheme 1).[4b,4d] **L2-b1** and **L2-b2** were obtained in a relatively

Scheme 1. Synthetic routes to (a) **L2-b1**, **L2-b2**, and (b) **DPA2**.
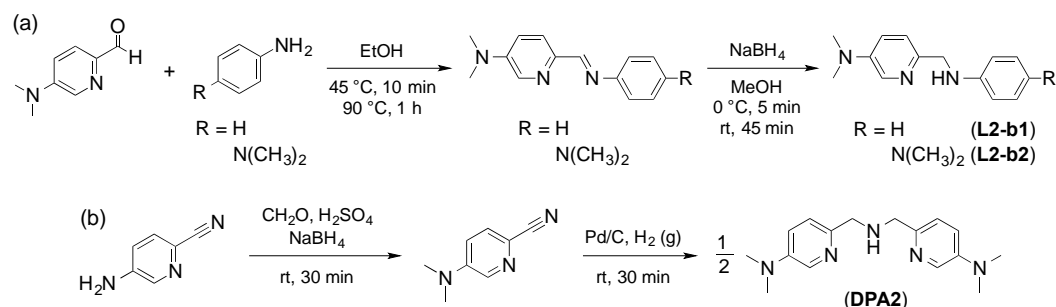
high yield through the formation of imine followed by its reduction to amine using sodium borohydride (NaBH₄).[4b,4d] In the case of **DPA2**, the reduction of the primary amino group on picolinonitrile to the dimethylamino functionality was carried out subsequently incorporating themselves to obtain the final product. Note that **PMA1**, **PMA2**, and **DPA1** are commercially available.

Influence on metal-free and metal-induced Aβ aggregation

The ability of our small molecules (Figure 1) to modulate Aβ aggregation in both the absence and presence of metal ions was monitored through inhibition and disaggregation experiments (reaction schemes of both studies shown in Figure 2a and Supporting Information, Figure S1a, respectively). The experiments were performed using $A\beta_{40}$ and $A\beta_{42}$, two major Aβ isoforms found in the AD-affected brain.[1a-c] The molecular weight (MW) distributions and morphological changes of the resultant Aβ species were analyzed by gel electrophoresis with Western blotting (gel/Western blot) and transmission electron microscopy (TEM), respectively.[4a-h] If a compound could

generate a variety of smaller Aβ species, the gel/Western blot would indicate significant smearing. The large aggregates produced upon treatment with a compound can be visualized by TEM, but are too large to penetrate into the gel matrix thus presenting very little smearing on the gel/Western blot (Figures 2, Supporting Information, Figure S1).

In inhibition experiments (analysis of compounds' effect on formation of Aβ aggregates, Figure 2a), various MW distributions of both metal-free $A\beta_{40}$ and metal–$A\beta_{40}$ species were displayed to different extents from the samples containing **L2-b2** (lane 2, Figure 2b) compared to compound-untreated peptides (lane C, Figure 2b). On the other hand, much less significant influence on Aβ aggregation was observed upon incubation with the other compounds (*i.e.*, **L2-b1**, **PMA1**, **PMA2**, **DPA1**, and **DPA2**) with and without metal ions. Moreover, similar to $A\beta_{40}$, both metal-free and metal-treated $A\beta_{42}$ aggregation pathways were altered by treatment with **L2-b2** (lane 2, Figure 2c), noticeably different from **L2-b1**, **PMA1**, **PMA2**, **DPA1**, and **DPA2**. In addition to gel/Western blot analyses, the morphologies of both metal-free $A\beta_{40}$/$A\beta_{42}$ and metal–$A\beta_{40}$/$A\beta_{42}$ aggregates produced upon
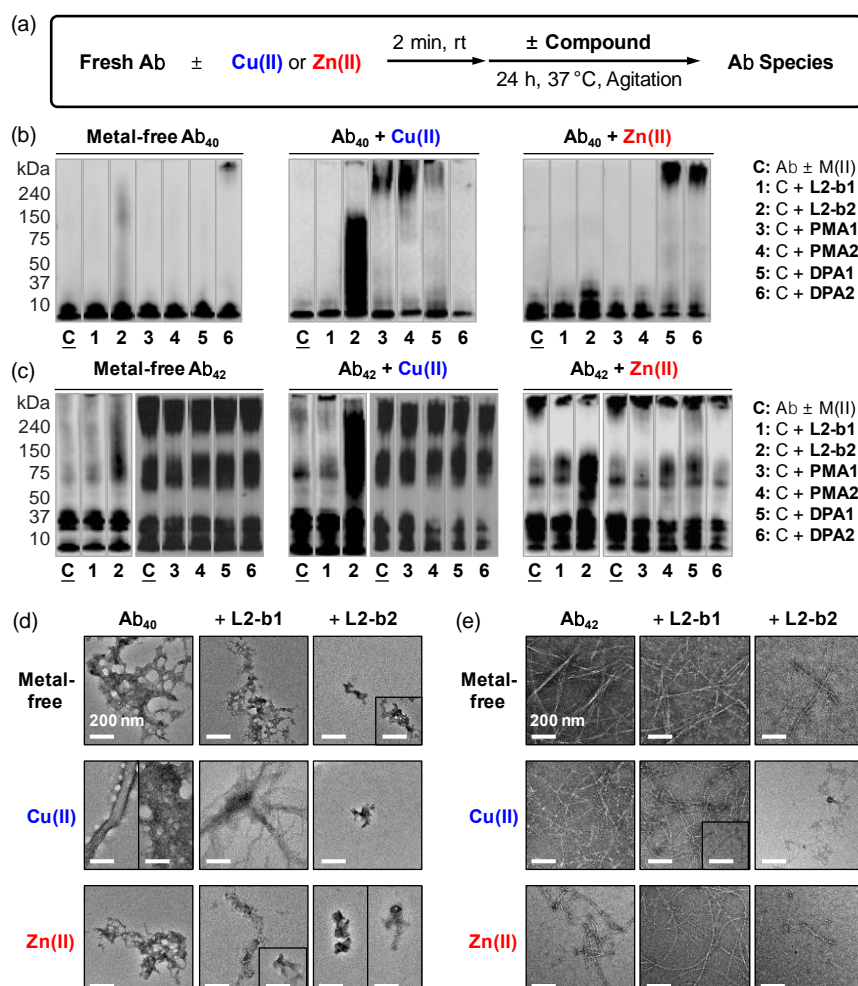

Figure 2. Effects of small molecules on formation of metal-free Aβ and metal–Aβ aggregates. (a) Scheme of the inhibition experiment. Visualization of MW distributions of resultant (b) $A\beta_{40}$ and (c) $A\beta_{42}$ species by gel/Western blot with an anti-Aβ antibody (6E10). Conditions: [Aβ] = 25 μM; [CuCl₂ or ZnCl₂] = 25 μM; [compound] = 50 μM; pH 6.6 (for Cu(II) experiments) or pH 7.4 (for metal-free and Zn(II) experiments); 37 °C; constant agitation. TEM images of the (d) $A\beta_{40}$ and (e) $A\beta_{42}$ samples from (b) and (c), respectively.

incubation with **L2-b1** or **L2-b2** were monitored by TEM. The resultant $A\beta_{40}$ and $A\beta_{42}$ aggregates generated by treatment with **L2-b2** were shown to be more amorphous aggregates and/or smaller fibrils than those obtained under compound-free and **L2-b1**-treated conditions (Figure 2d and 2e).

The results from disaggregation experiments (determination of the ability of compounds to disassemble preformed $A\beta$ aggregates; Supporting Information, Figure S1a) are similar to those from the inhibition studies (Supporting Information, Figure S1b-1e). Preformed metal-free $A\beta_{40}$ and metal-treated $A\beta_{40}$ aggregates incubated with **L2-b2** displayed various-sized peptide aggregates to different degrees (lane 2, Supporting Information, Figure S1b). Similar to inhibition experiments, **L2-b1**, **PMA1**, **PMA2**, **DPA1**, and **DPA2** could not detectably disaggregate preformed $A\beta_{40}$ aggregates or redirect their further aggregation under both metal-free and metal-present conditions (Supporting Information, Figure S1b). In the case of $A\beta_{42}$, **L2-b2** was also indicated to dismantle preformed metal-free and metal-treated $A\beta_{42}$ aggregates, distinct from the other compounds (Supporting Information, Figure S1c). Expected from the gel/Western blot studies, more noticeable morphological changes upon treatment of **L2-b2** to preformed metal-free and metal-bound $A\beta_{40}$/$A\beta_{42}$ aggregates were visualized, indicating more amorphous aggregates or thinner fibrils than the resultant $A\beta$ aggregates from compound-free and **L2-b1**-added samples (Supporting Information, Figure S1d and 1e).

Collectively, our gel/Western blot and TEM results suggest that structural variations of small molecules govern their distinct reactivities toward both metal-free and metal-induced $A\beta$ aggregation. **L2-b2**, which has the overall structure of **L2-b** with an additional dimethylamino group on the pyridine ring (Figure 1), is observed to redirect both metal-free $A\beta$ and metal–$A\beta$ aggregation pathways; however, **L2-b1** with the dimethylamino functionality, differently positioned from the backbone of **L2-b**, is not able to alter peptide aggregation regardless of the presence of metal ions. **PMA1** and **PMA2**, the metal chelating portions of **L2-b** and **L2-b1**/**L2-b2**, respectively (Figure 1), could not significantly control $A\beta$ aggregation in both the absence and presence of metal ions. In addition, **DPA1** and **DPA2** (Figure 1), the small molecules with the greater metal binding denticity and structural flexibility than **L2-b**, are not capable of distinguishably impacting $A\beta$ aggregation even in the presence of metal ions. Therefore, the results and observations from both the inhibition and disaggregation studies employing our chemical series validate that the overall framework of **L2-b** with the dimethylamino group(s) at proper position(s), instead of individual structural components, could achieve inhibitory reactivities of small molecules with metal-free $A\beta$ and/or metal–$A\beta$.

Biological activities

The capability of each compound to mediate cytotoxicity triggered by metal ions, metal-free $A\beta$, and metal–$A\beta$ was examined. More than *ca.* 85% of cell survival was exhibited when **L2-b1**, **L2-b2**, **PMA1**, **PMA2**, **DPA1**, and **DPA2** (up to 50 μM without metal ions; up to 25 μM with metal ions) were treated

to human neuroblastoma SK-N-BE(2)-M17 (M17) cells (Supporting Information, Figure S2). Additionally, the regulating activity of **L2-b2**, able to noticeably control both metal-free and metal-treated $A\beta$ aggregation (*vide supra*), against cytotoxicity induced by metal-free $A\beta$ or metal–$A\beta$ was further verified (Figure 3a). As shown in Figure 3a, our molecules in this study have relatively low toxicity in both the absence and presence of metal ions under conditions tested. Moreover, **L2-b2**, which has an additional dimethylamino group on **L2-b**'s backbone, is observed to possibly alleviate toxicity triggered by metal-free $A\beta$ and metal–$A\beta$ in living cells due to its abilities to modulate $A\beta$ aggregation (*vide supra*) and scavenge free radicals (*vide infra*).

The capability of **L2-b1**, **L2-b2**, **PMA1**, **PMA2**, **DPA1**, and **DPA2** to scavenge free radicals was measured by the Trolox (vitamin E analogue) equivalent antioxidant capacity (TEAC) assay which can evaluate compounds' capability of quenching ABTS cation radicals [ABTS$^{\bullet+}$; ABTS = 2,2'-azino-bis(3-ethylbenzothiazoline-6-sulfonic acid)] in both an organic solution (*i.e.*, EtOH) and a biologically relevant environment (*i.e.*, cell lysates).[4c-g,7] As shown in Figure 3b, the TEAC values of **L2-b1** and **L2-b2** [0.8 (± 0.1) and 1.9 (± 0.1) in EtOH; 0.7 (± 0.1) and 1.1 (± 0.1) in M17 lysates, respectively] were determined. The compound **L2-b2** presents a greater ability to quench free organic radicals than Trolox in both media, EtOH and cell lysates. The noticeable free organic radical scavenging ability of **L2-b1** and **L2-b2**, compared to **PMA1**, **PMA2**, **DPA1**, and **DPA2**,
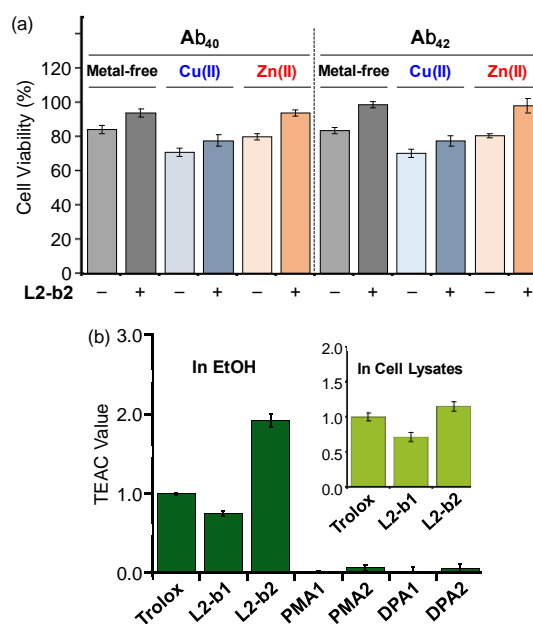

Figure 3. Biological activities of small molecules. (a) Viability of cells treated with **L2-b2** and $A\beta_{40}$ or $A\beta_{42}$ in the absence and presence of CuCl$_2$ or ZnCl$_2$. SK-N-BE(2)-M17 (M17) cells were incubated with metal-free $A\beta$ and metal–$A\beta$ followed by the addition of **L2-b2**. Cell viability (%) was determined by the MTT assay compared to cells treated with DMSO only (0–1%, v/v). Conditions: [$A\beta$] = 10 μM; [CuCl$_2$ or ZnCl$_2$] = 10 μM; [**L2-b2**] = 20 μM. (b) Free organic radical scavenging capability of **L2-b1**, **L2-b2**, **PMA1**, **PMA2**, **DPA1**, and **DPA2**, identified by the TEAC assay in EtOH or M17 cell lysates (inset). The TEAC values are relative to that of a vitamin E analogue, Trolox (6-hydroxy-2,5,7,8-tetramethylchroman-2-carboxylic acid). Error bars represent the standard error (SE) from three independent experiments (*P* < 0.05).

is expected from their relative lower IP values (*vide infra*, Figure 1). Together, the entire framework of **L2-b** (with and without additional dimethylamino group(s)) over individual structural portions is responsible for relative lower IP values that could offer the distinct scavenging activity of small molecules toward free radicals.

Mechanisms for modulating reactivities toward metal-free and metal-bound Aβ species

(i) Ionization potentials. The IPs of our small molecules (Figure 1) were calculated to anticipate the possibility of their modulating ability toward Aβ aggregation pathways and antioxidant capability. As depicted in Figure 1, **L2-b** and **L2-b2** are shown to have relatively lower IP values than the other structures (*i.e.*, **L2-b1**, **PMA1**, **PMA2**, **DPA1**, and **DPA2**) in both the gas and aqueous phases. Moreover, the singly occupied molecular orbitals (SOMOs) indicate that the structures of **L2-b** and **L2-b2**, composed of a dimethylamino group on the benzene ring, are observed to be more easily oxidized than that the structure with the dimethylamino functionality only on the pyridine ring (*i.e.*, **L2-b1**). Based on the IP values of our chemical series, oxidative transformations of the compounds (particularly, **L2-b** and **L2-b2**) could occur and subsequently direct their regulatory ability against Aβ peptides and free radicals (*vide supra*).

(ii) Metal binding. Cu^{II} or Zn^{II} binding of compounds was monitored by UV–vis or ^1H nuclear magnetic resonance (NMR) spectroscopy. Changes of the UV–vis spectra were observed upon addition of $CuCl_2$ to the EtOH solution of all small molecules (Figure 1), indicative of their binding to Cu^{II} (Supporting Information, Figure S3a-3f). In case of **L2-b1** and **L2-b2**, new optical bands were detected; for **PMA1** and **DPA1**, the intensity of the absorption spectra was increased; the spectral shifts of **PMA2** and **DPA2** were observed upon treatment with Cu^{II} (Supporting Information, Figure S3a-3f). Furthermore, Zn^{II} binding of compounds was investigated by UV–vis and ^1H NMR. The addition of Zn^{II} (1 equiv) to the CD_3CN solution of **L2-b1**, **PMA1**, or **PMA2** caused the variation of chemical shifts of the pyridyl protons suggesting the involvement of the N donor atoms on their pyridine ring in Zn^{II} binding (Supporting Information, Figure S3g-3i). In addition, the optical spectra of **L2-b2**, **DPA1**, and **DPA2** were altered upon introduction of Zn^{II} to their EtOH solution (Supporting Information, Figure S3j-3l). Together, our UV–vis and NMR studies present that our molecules can interact with Cu^{II} and Zn^{II}.

(iii) Interactions with metal-free and Zn^{II}-treated Aβ40 monomers. **L2-b2** is indicated to have its modulating ability toward both metal-free Aβ and metal–Aβ aggregation pathways, distinct from the other small molecules [particularly, **L2-b** (reactivity only for metal–Aβ species)[4b,4f] and **L2-b1** (no noticeable reactivity for both metal-free Aβ and metal–Aβ); Figure 2 and Supporting Information, Figure S1]. In order to pinpoint the different reactivity of these small molecules (*i.e.*, **L2-b**, **L2-b1**, **L2-b2**) toward targets, the interactions of **L2-b1** and **L2-b2** with monomeric Aβ40 in the absence of metal ions were
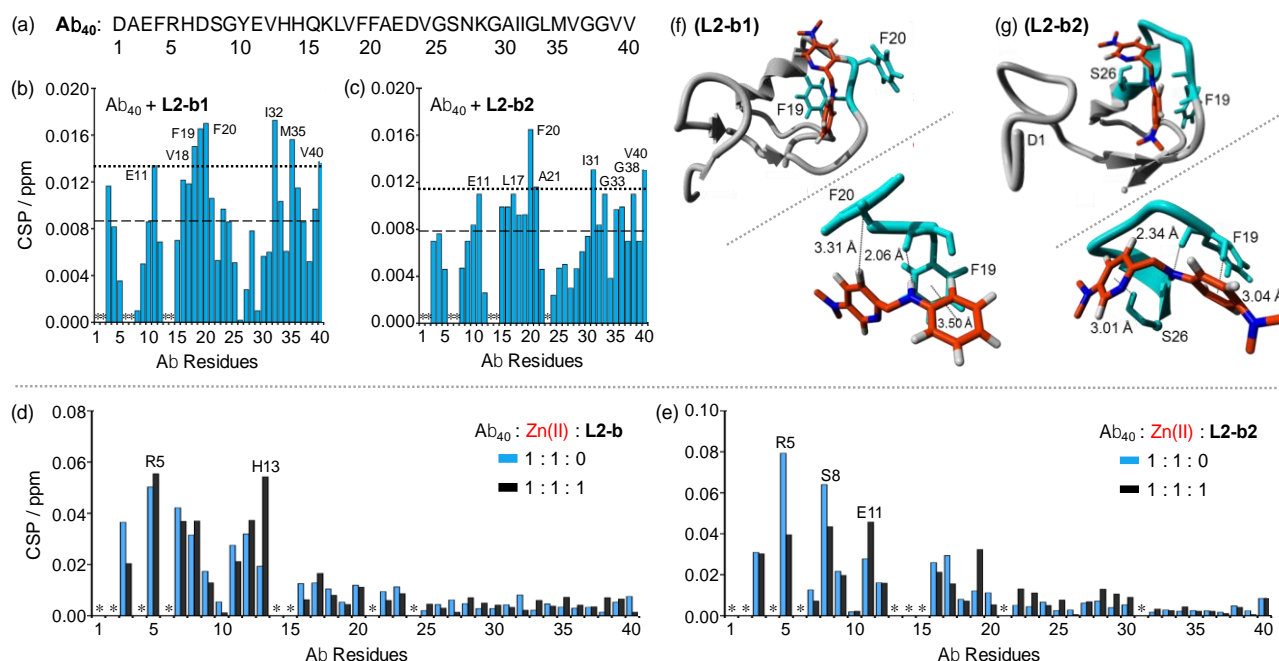

Figure 4. Interactions of **L2-b**, **L2-b1**, or **L2-b2** with metal-free or Zn^{II}-treated Aβ40 monomer. (a) Amino acid sequence of Aβ40. Plots of the chemical shift perturbation (CSP) determined through 2D ^1H–^{15}N SOFAST-HMQC NMR spectra of uniformly ^{15}N-labeled monomeric Aβ40 upon titration with (b) **L2-b1** or (c) **L2-b2**. The average CSP (dashed line) with standard deviation (dotted line) is presented. *Residues could not be resolved for analysis. Conditions: [Aβ40] = 80 μM; [**L2-b1** or **L2-b2**] = 0 or 800 μM; 20 mM PO_4, pH 7.4, 50 mM NaCl; 7% D_2O (v/v); 10 °C. Plots of the CSP obtained from 2D ^1H–^{15}N SOFAST-HMQC NMR spectra of uniformly ^{15}N-labeled monomeric Aβ40 upon addition of Zn(II) without (blue) and with (black) (d) **L2-b** or (e) **L2-b2**. *Residues could not be resolved for analysis. Conditions: [Aβ40] = 80 μM; [$ZnCl_2$] = 80 μM; [**L2-b** or **L2-b2**] = 80 μM; 20 mM PO_4, pH 7.4, 50 mM NaCl; 7% v/v D_2O. MD simulations showing interactions of (f) **L2-b1** or (g) **L2-b2** with monomeric Aβ40. Possible sites and energy of interactions of Aβ40 (PDB 1BA4) with **L2-b1** or **L2-b2** after all-atom MD simulations are summarized. The zoomed-in view (right, below) of each binding site with residues showing interaction distances labelled in Å with dashed lines (additional MD simulations data in Supporting Information, Figure S5).

first investigated by 2D band-selective optimized flip-angle short transient heteronuclear multiple quantum correlation (SOFAST-HMQC) NMR spectroscopy (Figure 4b, 4c and Supporting Information, Figure S4). Small but detectable chemical shifts were presented upon titration with 10 equiv of the compounds to metal-free Aβ_{40} monomer (Supporting Information, Figure S4). To identify the amino acid residues potentially involved in binding of compounds to the peptide, their chemical shift perturbation (CSP) was calculated (Figure 4b and 4c) indicating that **L2-b1** and **L2-b2** triggered slightly noticeable CSP at the residues [E11; L17-A21 (the self-recognition);[1c,1d] I31-G33, M35, G38, and V40 at the hydrophobic C-terminal region] to different degrees, relatively similar to **L2-b**.[4e] **L2-b1** and **L2-b2** resulted in the chemical shift of V40 at the C-terminus, like **L2-b**,[4e] which may reflect the rearrangement of the disordered C-terminus to pack against the compounds instead of direct or indirect interactions with Aβ_{40}. Overall, the compounds (*i.e.*, **L2-b1**, **L2-b2**, and **L2-b**[4e]) are observed to have weak interactions with metal-free Aβ.

To visualize the interactions between **L2-b**, **L2-b1**, or **L2-b2** and monomeric Aβ_{40} (PDB 1BA4),[8] studies *via* molecular docking and molecular dynamics (MD) simulations were conducted. Both rigid and flexible docking procedures were utilized using the Autodock Vina 1.5.6 program.[9] MD simulations were performed on the starting structure obtained from docking procedures on complexes of **L2-b**, **L2-b1**, or **L2-b2** with Aβ_{40}. These all-atom simulations were run by the GROMOS96 53a6 force field as implemented in the GROMACS program.[10] Multiple interactions of compounds with Aβ_{40} (*i.e.*, π–π interaction, C–H–π interaction, N–H–π interaction, hydrogen bonding) were observed (Figure 4f, 4g and Supporting Information, Figure S5). First, **L2-b** may interact with both polar and non-polar residues through hydrogen bonding between its secondary amine and H6 and π–π interactions between its benzene/pyridine rings and F4 or H14, respectively (Supporting Information, Figure S5a; left). Other amino acid residues of Aβ_{40} (*e.g.*, L17 and F19) were also shown to be involved in interactions with **L2-b** through hydrogen bonding and a π–π interaction, respectively (Supporting Information, Figure S5a; right). As shown in Figure 4f, **L2-b1** was held between two aromatic residues, F19 and F20, through π–π and C–H interactions, respectively. Additionally, hydrogen bonding between the backbone carbonyl O atom (between F19 and F20) and **L2-b1**'s secondary amine bridging the two aromatic rings could be generated. Three aromatic residues H6, Y10, and H14 might interact with **L2-b1** through a π–π interaction (Y10), a C–H–π interaction (H14), and hydrogen bonding (H6 and D7) (Supporting Information, Figure S5b; right).

The residues F19 and S26 were indicated to interact with **L2-b2** through C–H–π interactions (between **L2-b2**'s benzene ring and the H atom from the aromatic ring of F19; between **L2-b2**'s pyridine ring and the H atom from $^{\beta}$C of S26) (Figure 4g). Additionally, **L2-b2**'s secondary amine group and the backbone carbonyl O atom between F19 and F20 may form hydrogen bonding. Moreover, **L2-b2** could be held between two aromatic residues F4 and F20 *via* C–H–π (between its pyridine ring and

the H atom from the aromatic ring of F4) and N–H–π (between its secondary amine and F20) interactions, respectively. Hydrogen bonding between the N atom of dimethylamino group on **L2-b2**'s benzene ring and the backbone amine group of S8 could also be formed (Supporting Information, Figure S5c; right). For all binding modes, binding energies and contributions of electrostatic or hydrophobic interactions were calculated and summarized in the table (Supporting Information, Figure S5). Together, through MD simulations, the potential interactions of **L2-b**, **L2-b1**, and **L2-b2** with metal-free Aβ_{40} monomer could be envisioned. Based on our 2D NMR, MS, and MD simulations studies, the regulatory activity of molecules with metal-free Aβ may be achieved *via* the covalent adduct formation (observed by **L2-b2**; Figure 5b) rather than non-covalent interactions (*e.g.*, π–π and C–H–π interactions, hydrogen bonding).

The interaction of monomeric Aβ_{40} with **L2-b2** capable of controlling metal-free Aβ aggregation (*vide supra*; Figure 2 and Supporting Information, Figure S1) was further monitored by electrospray ionization mass spectrometry (ESI-MS) (Figure 5a, 5b and Supporting Information, Figure S6). Different from **L2-b** unable to interact with metal-free Aβ,[4b,4f] **L2-b2** or its degraded compounds [*e.g.*, *N,N*-dimethyl-*p*-phenylenediamine (**DMPD**) and/or oxidized **DMPD** (*i.e.*, cationic imine, **CI**;][4g] were shown to have interactions with metal-free Aβ (Figure 5b). When **L2-b2** was incubated with metal-free Aβ, a newly observed signal corresponding to the addition of 132 Da to Aβ, indicative of forming a covalent adduct of **CI**–Aβ, was exhibited (magenta, Figure 5b). This adduct could be generated *via* primary amine-containing residues from Aβ (*e.g.*, K16, K28) (Figure 5b and Supporting Information, Figure S6), similar to the complex formation of benzoquinone (**BQ**) with Aβ (**BQ**–Aβ)[4g] Such distinct interactions of **L2-b2** with Aβ (*i.e.*, the compounds' degradation and transformation followed by covalent cross-links with Aβ) could be associated with **L2-b2**-triggered alteration of metal-free Aβ aggregation, which was not observed from the samples of Aβ with **L2-b**.[4f]

For the interaction with Zn^{II}–Aβ, 2D NMR was employed to analyze the samples containing **L2-b** or **L2-b2** and Zn^{II}-bound uniformly ^{15}N-labeled Aβ_{40} monomer (Figure 4d, 4e and Supporting Information, Figure S7). **L2-b** induced relatively more CSP of R5 and H13 residues close to a metal binding site of Aβ_{40} (Figure 4d).[1b-d,3d,3e] As shown in Figure 4e, similar to **L2-b**, **L2-b2** caused CSP of residues, such as R5, S8, and E11, within proximity of the metal binding region. Thus, **L2-b** and **L2-b2** could interact with Zn^{II} surrounded by Aβ_{40} possibly leading to mediation of Zn^{II}–Aβ_{40} aggregation, as detected by gel/Western blot and TEM (Figure 2 and Supporting Information, Figure S1).

(iv) Interactions with metal-free and Zn^{II}-treated Aβ fibrils. Along with Aβ monomer, to verify how **L2-b** or **L2-b2** is able to disassemble preformed metal-free and/or metal-added Aβ aggregates to different extents, their interactions with metal-free and Zn^{II}-treated Aβ_{42} fibrils were studied by saturation transfer difference (STD) NMR (Figure 6a-6c). Signals in STD NMR are proportional to each atom of either **L2-b** or **L2-b2** to its macromolecular binding partner, fibrils, which allows atomic-level mapping of ligand binding to fibrillar Aβ.[11] In the case of
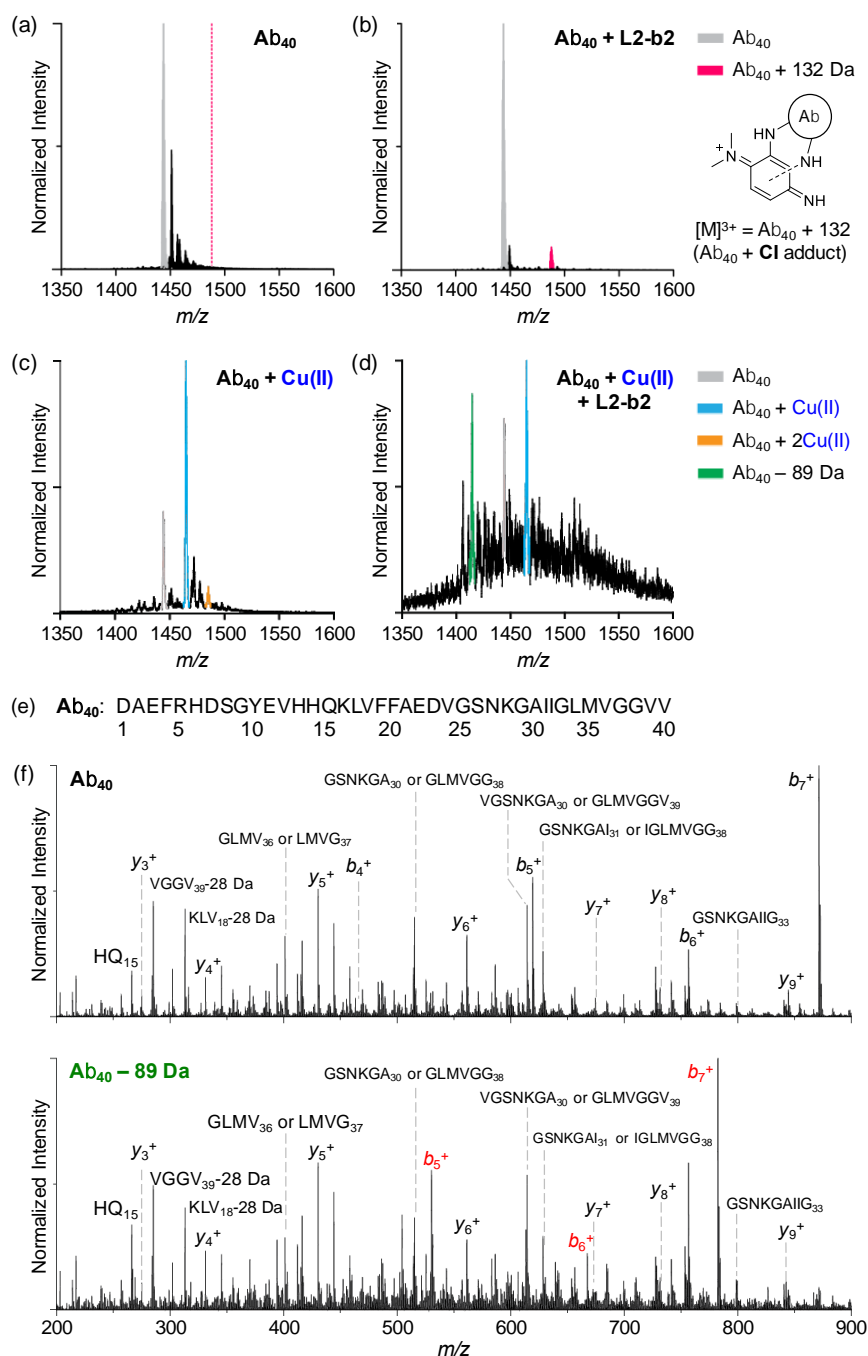
Figure 5. ESI-MS analysis of Aβ$_{40}$ incubated with **L2-b2** in the absence and presence of Cu^{II}. (a and b) The 3+ charge state of metal-free Aβ$_{40}$ with and without **L2-b2**. When **L2-b2** was treated with Aβ, the signal at *m/z* 1487.8 (131.97 Da increase from Aβ$_{40}$) possibly corresponding to an adduct formed with Aβ and oxidized **DMPD** (**Cl**; cleaved from **L2-b2**) was observed. Conditions: [Aβ$_{40}$] = 10 μM; [CuCl$_2$] = 10 μM; [**L2-b2**] = 50 μM; 20 mM ammonium acetate, pH 7.5; 37 °C; 6 h incubation; no agitation. The 3+ charge state of Aβ$_{40}$ incubated with (c) Cu^{II} or (d) both Cu^{II} and **L2-b2**. The signal highlighted in green corresponds to degraded Aβ by loss of 89.08 Da. Conditions: [Aβ$_{40}$] = 20 μM; [CuCl$_2$] = 20 μM; [**L2-b2**] = 120 μM; 100 mM ammonium acetate, pH 7.5; 37 °C; 30 min incubation; no agitation. (e) Amino acid sequence of Aβ$_{40}$. (f) MS/MS analyses of Aβ$_{40}$ with and without treatment of Cu^{II} and **L2-b2**. These data support that the amino acid sequence of Aβ is chemically modified within the first five residues (D$_1$A$_2$E$_3$F$_4$R$_5$) of the peptide in the presence of both Cu^{II} and **L2-b2**. All the Aβ$_{40}$ species containing the identified −89.08 Da covalent modification are highlighted in red, and are compared against control Aβ$_{40}$ MS/MS sequencing data acquired under the same conditions.

L2-b, the relatively strong saturation effect was observed at the pyridine ring with metal-free Aβ$_{42}$ fibrils with the slight saturation effect at the dimethylamino group. In addition to the pyridine ring, upon treatment of Zn^{II}–Aβ fibrils with **L2-b**, the relatively noticeable saturation effects on the molecule were also indicated at the methyl group between the pyridine ring and the secondary amine (Figure 6c; left). Different from **L2-b**, both two dimethylamino groups and the pyridine ring of **L2-b2** were
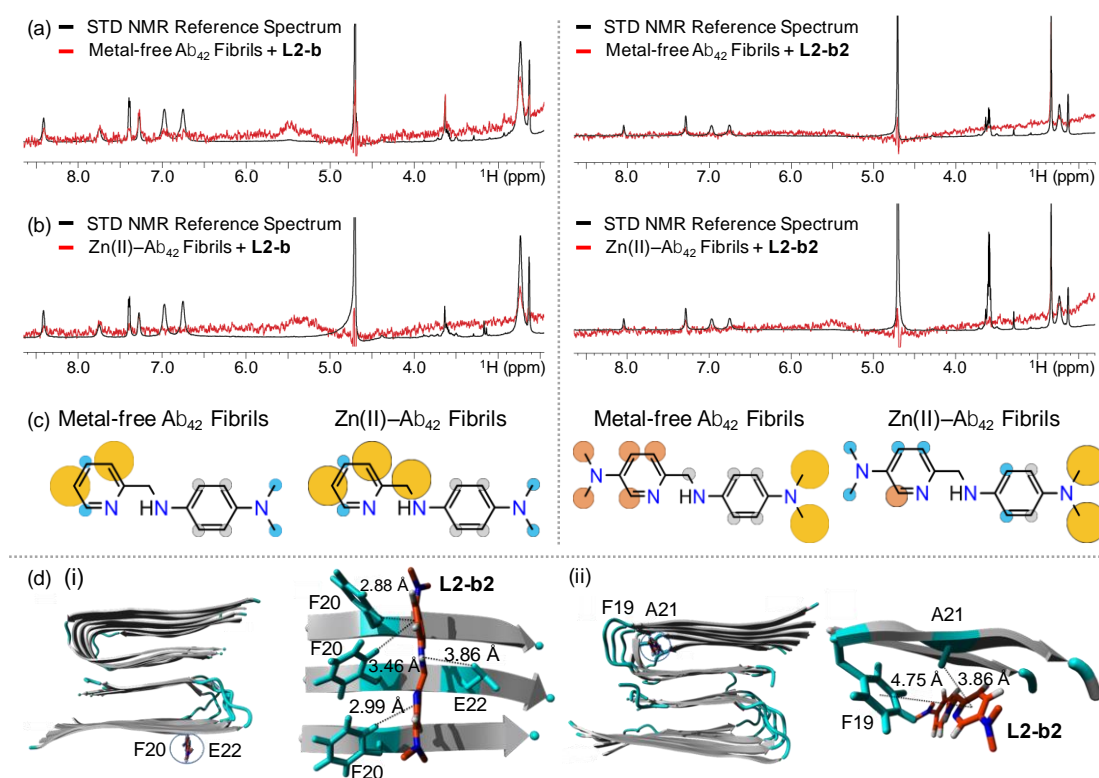
Figure 6. Interactions of **L2-b** or **L2-b2** with metal-free and Zn^{II}-treated Aβ fibrils. ^{1}H STD NMR spectra of **L2-b** (left) or **L2-b2** (right) in the presence (red) and absence (black) of (a) metal-free or (b) Zn^{II}-treated Aβ$_{42}$ fibrils. Comparison of the STD signal intensities (red) to the STD reference (black) reflects the relative proximity of the corresponding proton from the ligand to Aβ$_{42}$ fibrils. Conditions: [Aβ$_{42}$] = 2 μM; [ZnCl$_2$] = 2 μM; [**L2-b** or **L2-b2**] = 200 μM; 10 mM Tris-DCl, pD 7.4. (c) Normalized STD intensities mapped on to the structures of **L2-b** and **L2-b2** against metal-free Aβ$_{42}$ fibrils (left) and Zn^{II}–Aβ$_{42}$ fibrils (right). Yellow, orange, and blue circles indicate the STD effects of > 75%, 50–75%, and < 50%, respectively. Gray circles indicate the absence of the STD effect. (d) MD simulations showing interactions of **L2-b2** with metal-free Aβ$_{40}$ fibrils. Two potential binding sites (i and ii) of interaction of **L2-b2** with Aβ$_{40}$ fibrils (PDB 2LMN) after all-atom MD simulations. Right: The zoomed-in view of each binding site with residues showing interaction distances labelled in Å with dashed lines. Binding modes (for **L2-b**) and energies (for both **L2-b** and **L2-b2**) are presented in Supporting Information, Figure S8.

presented to have relatively significant saturation effects against metal-free Aβ$_{42}$ fibrils (Figure 6c; right), suggesting that this molecule could be relatively packed into the fibrillar conformation of Aβ, as described by a previously reported compound.[4d] When Zn^{II} was introduced to Aβ$_{42}$ fibrils, the saturation effects on the dimethylamino group of the pyridine ring was observed to be relatively less than those on that of the benzene ring, along with the reduced saturation influence on the pyridine ring.

To gain a better understanding of the interactions between Aβ fibrils (PDB 2LMN)[12] and **L2-b** or **L2-b2**, MD simulations were further conducted. As shown in Figure 6d and Supporting Information, Figure S8, two binding modes (*i.e.*, for both **L2-b** and **L2-b2**, alignment orthogonal to the surface of the β-strand; for **L2-b2**, intercalation into the loop of two β-strands) were observed. The complex of **L2-b** and fibrillar Aβ$_{40}$ formed hydrogen bonding of the H atoms from the benzene ring, the pyridine ring, and the secondary amine bridging two aromatic rings of **L2-b** with the O atoms from the carboxyl groups of E22s, as well as the N atom from the pyridine ring of **L2-b** with the H atom from aromatic ring of F20 (Supporting Information, Figure S8a). Additionally, a C–H–π interaction (between the H atom from the benzene ring of **L2-b** and the aromatic ring of F20) could stabilize the molecule to interact with Aβ fibrils (Supporting

Information, Figure S8a). In the case of **L2-b2**, this small molecule could be held on the fibril edge of the β-strand through a C–H–π interaction with F20 (between the pyridine/benzene rings of **L2-b2** and the H atoms from the aromatic rings of F20s). E22 may further assist in **L2-b2** binding to Aβ fibrils through hydrogen bonding formation between the H atom from the secondary amine between two aromatic rings of **L2-b2** and the O atom from the carbonyl group of E22 (Figure 6d(i)). Furthermore, **L2-b2** could be packed within the hydrophobic pocket of the fibril (intercalation into the loop of two β-strands) utilizing the interactions with A21 and F19 [C–H–π (between the pyridine ring of **L2-b2** and the H atom from the methyl group of A21) and π–π (between the pyridine ring of **L2-b2** and the aromatic ring of F19) interactions] (Figure 6d(ii)). This binding mode (packed by fibrils; intercalation) at the hydrophobic pocket, expected from STD NMR results (*vide supra*), may be linked to the relatively stronger direct interaction of **L2-b2** with preformed metal-free Aβ aggregates, as shown in a previously reported compound.[4d]

Taken together, STD NMR and MD simulations suggest how **L2-b** and **L2-b2** could interact with metal-free Aβ fibrils and Zn^{II}–Aβ fibrils. Through STD NMR, the metal binding portion of **L2-b** (**PMA1**; Figure 1) was observed to be related to the contact with

Zn^{II}–Aβ fibrils. In addition, different structural portions of **L2-b2** are indicated to have noticeable interactions with metal-free Aβ fibrils and Zn^{II}–Aβ fibrils. Furthermore, MD simulations visualize how such structural features of **L2-b** and **L2-b2** interact with Aβ fibrils, which suggests compounds' binding modes against peptide fibrils (especially, for **L2-b2**, alignment on the surface of the β-strand and intercalation into the loop that connects the two β-strands). Thus, the structural difference between **L2-b** and **L2-b2** (*i.e.*, additional dimethylamino group) is indicated to distinctly interact with metal-free and Zn^{II}-treated Aβ fibrils.

(v) Generation of degraded Aβ. In order to determine how **L2-b2** is able to alter Cu^{II}–Aβ aggregation, nano-ESI-MS (nESI-MS) optimized for the detection of non-covalent protein complexes was applied.[13] When the peptide was incubated with **L2-b2** in the presence of Cu^{II}, additional *m/z* signals corresponding to a mass loss of 89.08 (± 0.06) Da compared to apo Aβ$_{40}$ were detected (green signal, Figure 5d), similar to the results of **L2-b**.[4f] Tandem MS (MS/MS) sequencing indicates that this signal represents a modified form of Aβ$_{40}$ which lacks 89.08 Da from the first five residues of the N-terminus (D$_1$A$_2$E$_3$F$_4$R$_5$) (Figure 5e and 5f). These MS/MS data indicate that **L2-b2** likely binds to Aβ proximal to the binding site of Cu^{II}.[1b-d,3d,3e] Neither **L2-b2** nor Cu^{II} was directly detected in the complex with either the N-terminal cleavage product or apo Aβ$_{40}$ supporting the formation of a transient ternary complex consistent with previously published results.[4f] These data support that, compared to **L2-b**,[4f] the additional dimethylamino functionality on the pyridine ring is shown to still generate N-terminally cleaved Aβ species (loss of 89.08 Da) that could redirect Cu^{II}–Aβ aggregation. Along with the MS data (Figure 5d and 5f), compared to **L2-b**, these observations suggest that the additional dimethylamino moiety enables the compound (*i.e.*, **L2-b2**) to interact and react with both metal-free and Cu^{II}-bound Aβ.

(vi) Proposed mechanisms for reactivities of L2-b2 toward metal-free Aβ and metal–Aβ. Multiple mechanisms of **L2-b2** to redirect Aβ aggregation in the absence and presence of metal ions are proposed on the basis of our NMR, MS, and computational results. **L2-b2** could be cleaved through oxidative and hydrolytic processes generating transformed **DMPD** (**DMPD$_{transformed}$**)[4g] that can be covalently bound to Aβ monomers to form an Aβ–**DMPD$_{transformed}$** (Aβ–**CI**; Figure 5b) adduct. Upon Aβ–**CI** adduct formation, metal-free Aβ aggregation pathways could be redirected as previously reported.[4f] In addition, as shown in Figure 6, **L2-b2** could be intercalated between β-sheets of Aβ fibrils, which could be associated with its regulatory activity with metal-free Aβ fibrils, possibly similar to a previously reported molecule.[4d] In the presence of Zn^{II}, **L2-b2** is indicated to interact with monomeric Aβ (close to the metal binding site of Aβ)[1b-d,3d,3e] (Figure 4), which implies its potential contact with Zn^{II} surrounded by Aβ subsequently modulating peptide aggregation. More detailed studies of **L2-b2**'s interaction with Zn^{II}–Aβ are the subject of future studies. Lastly, toward Cu^{II}–Aβ, **L2-b2** is able to lead to Aβ degradation (Figure 5), similar to **L2-b**.[4f] This observed Aβ degradation could be related to the formation of a transient ternary complex between Aβ, Cu^{II}, and **L2-b2**, subsequently followed by **L2-b2**'s oxidation and Aβ degradation of by well-

known radical-mediated pathways.[14] Such degraded Aβ could lose aggregation propensity as full-length peptides.[4f] Based on analyses of Aβ products from both reactions of **L2-b2** with metal-free Aβ and Cu^{II}–Aβ, the oxidation of this molecule occurs, which suggests that its oxidative transformation is required for the desired reactivities with an emphasis on importance of anticipating IP values for rational design (Figure 1). Collectively, **L2-b2** is demonstrated to be a tool able to interact and react with all metal-free Aβ, Cu^{II}–Aβ, and Zn^{II}–Aβ to different extents *via* several disparate mechanisms.

Conclusions

Chemical tools capable of targeting and controlling individual or multiple pathogenic factors found in AD (*i.e.*, metals, metal-free and metal-bound Aβ, oxidative stress) have been developed to elucidate AD pathogenesis at the molecular level; however, such tool invention has been challenging. Unfortunately, a guideline of designing chemical tools for distinct targets (*e.g.*, as the first step, selecting key structural and mechanistic properties of tools) has not been established. To contribute to this foundation, a new class of small molecules was constructed based on the structure of **L2-b**, known as a chemical regulator for metal–Aβ,[4b,4f] with consideration of their BBB permeability and relatively low cytotoxicity. Employing our chemical series, the regulatory activities toward metal-free Aβ and metal–Aβ aggregation, along with free radical scavenging capability, are observed to be directed by compounds' structures (*e.g.*, functionality and entire backbone) as well as mechanistic characteristics (*e.g.*, covalent adduct formation with peptides and peptide degradation through compounds' transformations). Through our structure-mechanism-based design, a molecular multifunctional tool, **L2-b2**, was newly fashioned showing its abilities to regulate all of our desired targets (*i.e.*, metals, metal-free Aβ, metal–Aβ, and oxidative stress). Taken together, our overall multidisciplinary studies through a chemical library present a design concept of chemical tools toward individual or multiple inter-related pathological factors in AD based on structural and mechanistic details. Our structure-mechanism-based concept could open new avenues for devising chemical tools capable of regulating the actions of diverse pathological factors in human diseases. In principle, depending on different targets, distinct mechanisms of chemical tools to regulate their actions should be taken into account.

Experimental Section

Materials and methods

All reagents and solvents were purchased from commercial suppliers and used as received unless otherwise stated. **PMA1**, **PMA2**, and **DPA1** were purchased from Sigma-Aldrich (St. Louis, MO, USA). **L2-b**, **L2-b1**, **L2-b2**, and **DPA2** were synthesized as previously reported procedures (*vide infra*).[4b] Aβ$_{40}$ and Aβ$_{42}$ were purchased from AnaSpec (Fremont, CA, USA) (Aβ$_{42}$ = DAEFRHDSGYEVHHQKLVFFAEDVGSNKGAIIGLMV-GGVVIA). Double distilled H$_2$O (ddH$_2$O) was obtained from a Milli-Q Direct 16 system (Merck KGaA, Darmstadt, Germany). An Agilent 8453

UV–visible (UV–vis) spectrophotometer (Santa Clara, CA, USA) was used to measure optical spectra. TEM images were taken using a JEOL JEM-2100 transmission electron microscope (UNIST Central Research Facilities, Ulsan, Republic of Korea). Absorbance values for biological assays, including the MTT and TEAC assays, were measured on a SpectraMax M5e microplate reader (Molecular Devices, Sunnyvale, CA, USA). NMR studies of Aβ with compounds in both the absence and presence of Zn^{II} were carried out on a 900 MHz Bruker spectrometer equipped with a cryogenic probe (Michigan State University in Lansing, MI, USA). A Waters (Milford, MA) Synapt G2 HDMS equipped with a nano-electrospray ionization (nESI) or ESI source (Waters, Milford, MA, USA) was used to study complex formation between **L2-b2** and Aβ$_{40}$ with and without Cu^{II}.

[1] a) R. Jakob-Roetne, H. Jacobsen, *Angew. Chem. Int. Ed.* **2009**, *48*, 3030-3059; b) K. P. Kepp, *Chem. Rev.* **2012**, *112*, 5193-5239; c) C. Rodriguez-Rodriguez, M. Telpoukhovskaia, C. Orvig, *Coord. Chem. Rev.* **2012**, *256*, 2308-2332; d) M. W. Beck, A. S. Pithadia, A. S. DeToma, K. J. Korshavn, M. H. Lim in *Ligand Design in Medicinal Inorganic Chemistry* (Ed.: T. Storr), Wiley, Chichester, **2014**, Chapter 10, pp. 256-286.

[2] a) K. Ono, M. M. Cordron, D. B. Teplow, *Proc. Natl. Acad. Sci. USA* **2009**, *106*, 14745-14750; b) C. Haass, D. J. Selkoe, *Nat. Rev. Mol. Cell Biol.* **2007**, *8*, 101-112; c) K. P. Kepp, *J. Alzheimers Dis.* **2016**, *56*, 1-11.

[3] a) J. A. Duce, A. I. Bush, *Prog. Neurobiol.* **2010**, *92*, 1-18; b) E. L. Que, D. W. Domaille, C. J. Chang, *Chem. Rev.* **2008**, *108*, 1517-1549; c) P. Zatta, D. Drago, S. Bolognin, S. L. Sensi, *Trends Pharmacol. Sci.* **2009**, *30*, 346-355; d) P. Faller, *ChemBioChem* **2009**, *10*, 2837-2845; e) S.

Chassaing, F. Collin, P. Dorlet, J. Gout, C. Hureau, P. Faller, *Curr. Top. Med. Chem.* **2012**, *12*, 2573-2595; f) A. A. Belaidi, A. I. Bush, *J. Neurochem.* **2016**, *139*, 179-197.

[4] a) S. S. Hindo, A. M. Mancino, J. J. Braymer, Y. Liu, S. Vivekanandan, A. Ramamoorthy, M. H. Lim, *J. Am. Chem. Soc.* **2009**, *131*, 16663-16665; b) J.-S. Choi, J. J. Braymer, R. P. Nanga, A. Ramamoorthy, M. H. Lim, *Proc. Natl. Acad. Sci. USA* **2010**, *107*, 21990-21995; c) J. S. Derrick, R. A. Kerr, K. J. Korshavn, M. J. McLane, J. Kang, E. Nam, A. Ramamoorthy, B. T. Ruotolo, M. H. Lim, *Inorg. Chem.* **2016**, *55*, 5000-5013; d) S. Lee, X. Zheng, J. Krishnamoorthy, M. G. Savelieff, H. M. Park, J. R. Brender, J. H. Kim, J. S. Derrick, A. Kochi, H. J. Lee, C. Kim, A. Ramamoorthy, M. T. Bowers, M. H. Lim, *J. Am. Chem. Soc.* **2014**, *136*, 299-310; e) M. G. Savelieff, Y. Liu, R. R. Senthamarai, K. J. Korshavn, H. J. Lee, A. Ramamoorthy, M. H. Lim, *Chem. Commun.* **2014**, *50*, 5301-5303; f) M. W. Beck, S. B. Oh, R. A. Kerr, H. J. Lee, S. H. Kim, S. Kim, M. Jang, B. T. Ruotolo, J. Y. Lee, M. H. Lim, *Chem. Sci.* **2015**, *6*, 1879-1886; g) J. S. Derrick, R. A. Kerr, Y. Nam, S. B. Oh, H. J. Lee, K. G. Earnest, N. Suh, K. L. Peck, M. Ozbil, K. J. Korshavn, A. Ramamoorthy, R. Prabhakar, E. J. Merino, J. Shearer, J. Y. Lee, B. T. Ruotolo, M. H. Lim, *J. Am. Chem. Soc.* **2015**, *137*, 14785-14797; h) A. K. Sharma, S. T. Pavlova, J. Kim, D. Finkelstein, N. J. Hawco, N. P. Rath, J. Kim, L. M. Mirica, *J. Am. Chem. Soc.* **2012**, *134*, 6625-6636; i) C. Rodriguez-Rodriguez, N. Sanchez de Groot, A. Rimola, A. Alvarez-Larena, V. Lloveras, J. Vidal-Gancedo, S. Ventura, J. Vendrell, M. Sodupe, P. Gonzalez-Duarte, *J. Am. Chem. Soc.* **2009**, *131*, 1436-1451.

[5] H. F. Kung, C. W. Lee, Z. P. Zhuang, M. P. Kung, C. Hou, K. Plossl, *J. Am. Chem. Soc.* **2001**, *123*, 12740-12741.

[6] a) A. Avdeef, S. Bendels, L. Di, B. Faller, M. Kansy, K. Sugano, Y. Yamauchi, *J. Pharm. Sci.* **2007**, *96*, 2893-2909; b) *BBB Protocol and Test Compounds*, *pI*ON Inc., **2009**.

[7] a) R. Re, N. Pellegrini, A. Proteggente, A. Pannala, M. Yang, C. Rice-Evans, *Free Radic. Biol. Med.* **1999**, *26*, 1231-1237; b) H. Schugar, D. E. Green, M. L. Bowen, L. E. Scott, T. Storr, K. Bohmerle, F. Thomas, D. D. Allen, P. R. Lockman, M. Merkel, K. H. Thompson, C. Orvig, *Angew. Chem. Int. Ed.* **2007**, *46*, 1716-1718.

[8] M. Coles, W. Bicknell, A. A. Watson, D. P. Fairlie, D. J. Craik, *Biochemistry* **1998**, *37*, 11064-11077.

[9] O. Trott, A. J. Olson, *J. Comput. Chem.* **2010**, *31*, 455-461.

[10] a) C. Oostenbrink, A. Villa, A. E. Mark, W.F. Van Gunsteren, *J. Comput. Chem.* **2004**, *25*, 1656-1676; b) D. A. Case, T. E. Cheatham III, T. Darden, H. Gohlke, R. Luo, K. M. Merz Jr., A. Onufriev, C. Simmerling, B. Wang, R. J. Woods, *J. Comput. Chem.* **2005**, *26*, 1668-1688; c) E. Lindahl, B. Hess, *J. Mol. Model* **2001**, *7*, 306-317.

[11] M. Mayer, B. Meyer, *J. Am. Chem. Soc.* **2001**, *123*, 6108-6117.

[12] A. T. Petkova, W. M. Yau, R. Tycko, *Biochemistry* **2006**, *45*, 498-512.

[13] a) H. Hernandez, C. V. Robinson, *Nat. Protoc.* **2007**, *2*, 715-726; b) G. R. Hilton, J. L. Benesch, *J. R. Soc. Interface.* **2012**, *9*, 801-816.

[14] a) C. L. Hawkins, M. J. Davies, *Biochim. Biophys. Acta* **2001**, *1504*, 196-219; b) W. M. Garrison, Chem. Rev. 1987, 87, 381-398; c) M. R. Porter, A. Kochi, J. A. Karty, M. H. Lim, M. J. Zaleski, *Chem. Sci.* **2015**, *6*, 1018-1026; d) M. W. Beck, J. S. Derrick, R. A. Kerr, S. B. Oh, W. J. Cho, S. J. C. Lee, Y. Ji, J. Han, Z. S. Tehrani, N. Suh, S. Kim, S. D. Larsen, K. S. Kim, J.-Y. Lee, B. T. Ruotolo M. H. Lim, *Nat. Commun.* **2016**, *7*, 13115.

FULL PAPER

Inventing smart chemical tools:

A structure-mechanism-based design strategy is demonstrated to be useful for inventing chemical tools able to regulate the actions of diverse pathological factors in Alzheimer's disease.
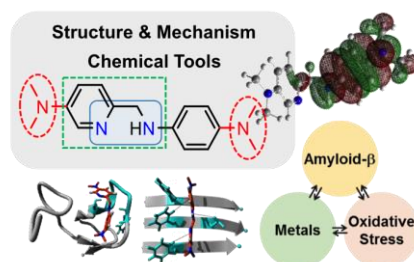
Dr. Hyuck Jin Lee, Kyle J. Korshavn, Younwoo Nam, Thomas J. Paul, Dr. Richard A. Kerr, Dr. Il Seung Youn, Juhye Kang, Dr. Mehmet Ozbil, Prof. Dr. Kwang S. Kim, Prof. Dr. Brandon T. Ruotolo, Prof. Dr. Rajeev Prabhakar,* Prof. Dr. Ayyalusamy Ramamoorthy* and Prof. Dr. Mi Hee Lim*

Page No. – Page No.

Structural and Mechanistic Insights into Development of Chemical Tools to Control Individual and Inter-related Pathological Features in Alzheimer's Disease

Author Manuscript

Table of Contents

Author Manuscript

Experimental Section

Synthesis of L2-b1. L2-b1 was synthesized with slight modifications of a previously reported method.[1] Aniline (150 mg, 1.6 mmol) was dissolved in 15 mL of EtOH (treated with molecular sieves overnight) followed by addition of 5-dimethylamino-2-pyridinecarboxaldehyde (285 mg, 1.9 mmol). The reaction solution was allowed to stir at 45 °C for 10 min and its temperature was increased to 90 °C. After 1 h, the solution was cooled down to room temperature and concentrated until precipitates were formed. The resulting solid precipitates were then dissolved in dry MeOH and cooled to 0 °C in a N_2-purged round-bottom flask. To the solution, sodium borohydride ($NaBH_4$; 307 mg, 8.1 mmol) was slowly introduced at 0 °C for 5 min. After warming up to room temperature, the resulting solution was further stirred for 45 min. The reaction mixture was then quenched with water, extracted three times with dichloromethane (CH_2Cl_2), washed once with brine, and concentrated. The crude products were purified by column chromatography (SiO_2; EtOAc:Et_3N 100:0.1; R_f = 0.54) followed by recrystallization with Et_2O and hexanes (260 mg, 1.1 mmol, 71%). ^{1}H NMR (400 MHz, CD_2Cl_2) / δ (ppm): 8.10 (2H, d, J = 3.0 Hz), 7.15 (3H, m), 7.00 (2H, dd, J = 8.6, 3.0 Hz), 6.66 (3H, m), 4.75 (1H, s (broad)), 4.30 (2H, d, J = 5.3 Hz), 2.95 (6H, s). ^{13}C NMR (100 MHz; CD_2Cl_2) / δ (ppm): 149.0, 146.2, 146.0, 134.7, 129.6, 122.0, 120.0, 117.5, 113.4, 49.0, 40.6. HRMS: Calcd for $[M+H]^+$, 228.3190; found, 228.3192.

Synthesis of L2-b2. L2-b2 was synthesized with slight modifications of a previously reported method.[1] **DMPD** (50 mg, 0.4 mmol) was added into a flame-dried flask under N_2 (g) and then dissolved in 10 mL of EtOH (treated with molecular sieves overnight). 5-Dimethylamino-2-pyridinecarboxaldehyde (70 mg, 0.5 mmol) was introduced and stirred at 45 ºC for 10 min and

90 ℃ for 1 h. The resulting solution was allowed to cool to room temperature, and the solvent was removed *in vacuo*. Dry MeOH was added to the flask under N_2 (g) and cooled down to 0 °C. A portion of NaBH$_4$ (70 mg, 1.9 mmol) was slowly introduced at 0 °C for 5 min followed by stirring for 45 min at room temperature. The reaction mixture was then quenched with water, extracted three times with CH_2Cl_2, washed once with brine, and concentrated. The crude products were purified by column chromatography (SiO$_2$; EtOAc:Et$_3$N 100:1; R_f = 0.29; 68 mg, 0.3 mmol, 70%). ^{1}H NMR (400 MHz, CD$_2$Cl$_2$) / δ (ppm): 8.09 (1H, d, J = 3.0 Hz), 7.15 (1H, d, J = 8.6 Hz), 6.99 (1H, dd, J = 8.6, 3.0 Hz), 6.69 (2H, d, J = 8.9 Hz), 6.62 (2H, d, J = 8.9 Hz), 4.25 (1H, s (broad)), 2.95 (6H, s), 2.79 (6H, s). ^{13}C NMR (100 MHz; CD$_2$Cl$_2$) / δ (ppm): 147.0, 145.8, 14.6, 141.4, 134.8, 122.1, 120.0, 116.0 114.8, 50.1, 42.4, 40.6. HRMS: Calcd for $[M+H]^+$, 271.3880; found, 271.3879.

Synthesis of DPA2. DPA2 was synthesized with slight modifications of a previously reported method.[2] 5-(Dimethylamino)picolinonitrile (100 mg, 0.7 mmol) was added into a flame-dried round-bottom flask (100 mL) containing dry MeOH (20 mL). Pd/C (10 wt %; 150 mg, 1.6 mmol) was added to the resulting mixture at room temperature. The solution was stirred under N_2 (g) for 10 min and then H_2 (g) for 5 or 6 h at room temperature. The Pd/C residues were filtered through the Celite and washed with cold MeOH (2 x 15 mL). To collected MeOH solution was slowly treated with 4 M HCl (0.4 mL) affording the light yellow solution. The mixture was concentrated *in vacuo* showing light yellow precipitates that were purified by column chromatography (SiO$_2$; MeOH:CH$_2$Cl$_2$ = 1:10; R_f = 0.70) followed by recrystallization with MeOH and Et$_2$O. The final product was washed with CH$_2$Cl$_2$ and Et$_2$O (65.9 mg, 0.2 mmol, 66%). ^{1}H NMR (400 MHz, CD$_3$OD) / δ (ppm): 8.25 (2H, d, J = 3.1 Hz), 8.07 (2H, d, J = 9.2 Hz), 7.83 (2H, dd, J = 4.6, 1.6

Hz), 4.68 (4H, s), 3.18 (12H, s). ^{13}C NMR (100 MHz; CD$_3$OD) / δ (ppm): 149.7, 130.7, 130.4, 127.4, 126.4, 47.8, 40.3. HRMS: Calcd for [M+H]$^+$, 286.2032; found, 286.2030.

Parallel Artificial Membrane Permeability Assay for the Blood-Brain Barrier (PAMPA-BBB). PAMPA-BBB experiments of compounds were carried out using the PAMPA Explorer kit (*p*ION, Inc. Billerica, MA, USA) with modifications to previously reported protocols.[1-3] Each stock solution was diluted with Prisma HT buffer (pH 7.4, *p*ION) to a final concentration of 25 μM (1% v/v final DMSO concentration). The resulting solution was added to the wells of the donor plate (200 μL, number of replicates = 12). BBB-1 lipid formulation (5 μL, *p*ION) was used to coat the polyvinylidene fluoride (PVDF, 0.45 μM) filter membrane on the acceptor plate. This acceptor plate was placed on top of the donor plate forming a sandwich. Brain sink buffer (BSB, 200 μL, *p*ION) was added to each well of the acceptor plate. The sandwich was incubated for 4 h at room temperature without stirring. UV−vis spectra of the solutions in the reference, acceptor, and donor plates were measured using a microplate reader. The PAMPA Explorer software [v. 3.8 (*p*ION)] was used to calculate the value of $-\log P_e$ for each compound. CNS± designations were assigned by comparison to compounds that were identified in previous reports.[4]

Aβ Aggregation Studies. Experiments with Aβ were conducted according to previously published methods.[1,2,3a,3b] To prepare Aβ peptides, either Aβ$_{40}$ or Aβ$_{42}$ was dissolved in ammonium hydroxide (NH$_4$OH, 1% v/v, aq), aliquoted, lyophilized overnight, and stored at −80 °C. For the experiments, a stock solution of Aβ was prepared by dissolving the lyophilized peptide in 1% NH$_4$OH and diluting with ddH$_2$O. The concentration of Aβ peptides in the

S5

solution was determined by measuring the absorbance of the solution at 280 nm (ε = 1450 M^{-1}cm^{-1} for Aβ_{40}; ε = 1490 M^{-1}cm^{-1} for Aβ_{42}). The peptide stock solution was diluted to a final concentration of 25 μM in the chelex-treated buffered solution containing HEPES [4-(2-hydroxyethyl)-1-piperazineethanesulfonic acid] (20 μM) (pH 6.6 for Cu(II) samples; pH 7.4 for metal-free and Zn(II) samples) and NaCl (150 μM). For inhibition studies, **L2-b1**, **L2-b2**, **PMA1**, **PMA2**, **DPA1**, or **DPA2** [50 μM; 1% v/v DMSO] was added to the sample of Aβ (25 μM) in the absence and presence of a metal chloride (CuCl$_2$ or ZnCl$_2$; 25 μM) followed by incubation at 37 °C with constant agitation for 24 h. For disaggregation studies, Aβ with and without metal ions was incubated for 24 h at 37 °C with constant agitation. **L2-b1**, **L2-b2**, **PMA1**, **PMA2**, **DPA1**, or **DPA2** (50 μM; 1% v/v DMSO) was added afterward to the solution containing Aβ aggregates, and incubated for additional 24 h at 37 °C.

Gel Electrophoresis and Western Blot. Each sample (10 μL) from both inhibition and disaggregation experiments was separated on a 10–20% Tris-tricine gel (Invitrogen, Grand Island, NY, USA) and transferred onto nitrocellulose membrane which was blocked with bovine serum albumin (BSA) solution (3% w/v; Sigma) in Tris-buffered saline containing 0.1% Tween-20 (TBS-T) for 2 h at room temperature. Then, the membranes were incubated with a primary antibody (6E10, Covance, Princeton, NJ, USA; 1:2,000) in a solution of 2% w/v BSA (in TBS-T) overnight at 4 °C. After washing with TBS-T three times (10 min each), the horseradish peroxidase-conjugated goat anti-mouse secondary antibody (1:5,000; Cayman Chemical Company) in 2% BSA (in TBS-T) was added to the membrane and incubated for 1 h at room temperature. SuperSignal West Pico Chemiluminescent Substrate (Thermo Scientific, Rockford, IL, USA) was used to visualize protein bands.

S6

Transmission Electron Microscopy (TEM). Samples for TEM were prepared according to previously reported methods.[1,2,3a,3b] Glow-discharged grids (Formar/Carbon 300-mesh, Electron Microscopy Sciences, Hatfield, PA, USA) were treated with samples from inhibition and disaggregation experiments (5 μL) for 2 min at room temperature. Excess sample was removed carefully with filter paper and washed twice with ddH$_2$O. Each grid was treated with uranyl acetate (1% w/v ddH$_2$O, 5 μL) for 1 min. Excess stain was blotted off and the grids were air dried for at least 20 min at room temperature. Images from each sample were taken on a JEOL JEM-2100 TEM (200 kV) at 25,000x magnification.

Calculation of Ionization Potentials (IPs). First-principles calculations using Gaussian09[5] were carried out. The geometry optimization was performed using the M06/6-31G(d) level of theory for both neutral and ionized forms of each molecule. Thermodynamic parameters were only considered to calculate ionization potentials due to the difficulty of computing the kinetics of electron transfer steps. The thermodynamic parameters were calculated at the M06/6-311+G(2df,2p) level of theory at gas and solvent (water) phases (using polarizable continuum model), respectively.

2D NMR. The interaction of Aβ$_{40}$ with **L2-b1** or **L2-b2** was monitored by 2D ^{1}H-^{15}N band-selective optimized flip-angle short transient heteronuclear multiple quantum correlation (SOFAST-HMQC) NMR at 10 °C.[6] Uniformly ^{15}N-labeled Aβ$_{40}$ (rPeptide, Bogart, GA, USA) was first dissolved in 1% NH$_4$OH and lyophilized. The peptide was redissolved in 3 μL of DMSO-*d$_6$* (Cambridge Isotope, Tewksbury, MA, USA) and diluted with phosphate buffer, NaCl, D$_2$O, and ddH$_2$O to a final peptide concentration of 80 μM (20 mM PO$_4$, pH 7.4, 50 mM NaCl; 7%

v/v D_2O). Each spectrum was obtained using 64 complex t_1 points and a 0.1 s recycle delay on a Bruker Avance 600 MHz NMR spectrometer. The 2D data were processed using TOPSPIN 2.1 (from Bruker). Resonance assignment was performed with SPARKY 3.1134 using published assignments for $A\beta_{40}$ as a guide.[6,7]

Saturation Transfer Difference (STD) NMR. For STD NMR experiments, a solution of fibrillar $A\beta_{42}$ (150 μM) was prepared through incubation for 24 h at 37 °C with constant agitation in 10 mM Tris-DCl at pD 7.4 (corrected for the isotope effect) containing 95% D_2O with or without $ZnCl_2$ (150 μM). The samples for STD experiments were prepared by diluting fibrils to 2 μM (effective monomer concentration) into 10 mM deuterated Tris-DCl to which 200 μM of compound (0.5% DMSO-d_6) was added. STD experiments were acquired with a train of 50 dB Gaussian-shaped pulses of 0.049 sec with an interval of 0.001 sec at either −1.0 ppm (on resonance)[8] or 40 ppm (off resonance) with a total saturation time of 2 sec on a Bruker 600 MHz NMR spectrometer.[3b,9] 1024 scans were recorded for the STD spectrum, and 512 scans were recorded for the reference spectrum at 25 °C. An inter-scan delay of 1 sec was used for both the STD and the reference experiments.

Mass Spectrometric Analyses. All mass spectrometric experiments with Aβ were carried out on a Synapt G2 (Waters, Manchester, UK). Two different ionization methods, electrospray (ESI) and nano-electrospray ionization (nESI), were applied. (a) By ESI, $A\beta_{40}$ (100 μM) was prepared with a compound [**L2-b** or **L2-b2** (500 μM)] in 20 mM ammonium acetate (pH 7.5) with and without the addition of $CuCl_2$ (100 μM). Prepared samples were incubated at 37 °C for 6 h (for metal-free samples) and 1 h [for Cu(II)-containing samples] without agitation. Incubated samples

were diluted by 10-fold before mass spectrometric analysis. The capillary voltage, sampling cone voltage, and source temperature were adjusted to 2.8 kV, 70 V, and 40 °C, respectively. (b) Samples were ionized using a nano-electrospray source operated in the positive ion mode. MS instrumentation was operated at a backing pressure of 2.7 mbar and sample cone voltage of 40 V. The *m/z* scale was calibrated using aqueous cesium iodide (20 mg/mL). For peptide-derivative-metal ligation studies, aliquots of $A\beta_{40}$ peptides (final concentration, 20 μM) were sonicated for 5 sec prior to incubation with or without a source of Cu(II) [copper(II) acetate; 20 μM] at 37 °C for 10 min. After the initial incubation, samples were titrated against a source of the ligand (final concentration: 0, 20, 40 and 120 μM) and incubated at 37 °C for 30 min prior to analysis. Solution conditions were 100 mM ammonium acetate (pH 7.5) with 1% v/v DMSO. Accurate mass values for covalently modified complexes were calculated using the monoisotopic peak difference between apo and modified states with errors reported as a function of two times the standard deviation. All other conditions are consistent with previously published methods.[10]

Molecular Dynamics (MD) Simulations. Molecular docking procedures were performed using the Autodock Vina 1.5.6[11] software to investigate the binding of **L2-b**, **L2-b1**, and **L2-b2** to the $A\beta_{40}$ monomer and fibril. All three molecular docking methods were utilized: (i) rigid docking, (ii) flexible docking, and (iii) rigid docking on different conformations of fibrils. Since the flexibility of the receptor (the Aβ monomer and fibril) was absent in rigid docking, multiple structures of the Aβ fibrils derived from short-term 5 ns molecular dynamics (MD) simulations in an aqueous solution were used in the third method of docking. Furthermore, due to the flexibility of the monomer, a long 100 ns MD simulation was run on the peptide alone. The size of the grid was chosen to cover the whole ligand−protein complex, and the spacing was kept to

S9

1.00 Å which is a standard value for Autodock Vina. Each docking trial produced 20 poses with an exhaustiveness value equal to 20. Snapshots were taken every nanosecond to allow for docking to different monomeric Aβ_{40} conformations. 20 poses were obtained for each snapshot taken, totaling 2000 poses. Starting structures for MD simulations were chosen based on residue binding abundances obtained by careful analysis of the docked poses.

The MD simulations of **L2-b**, **L2-b1**, or **L2-b2** bound to Aβ monomers or fibrils were performed using the GROMACS program utilizing the GROMOS force field GROMOS96 53A6.[12] For the monomer, unrestrained 25 ns, all-atom MD simulations were performed, where the first 5 ns of the simulation was part of the pre-production phase followed by 20 ns of a production phase. For the fibril, unrestrained 50 ns, all-atom MD simulations were carried out. For all simulations, the starting structures were placed in a cubic box with dimensions of 40 × 40 × 40 Å for monomeric Aβ_{40} (PDB 1BA4[13]) and 74 × 60 × 50 Å for the 2-fold fibrils (PDB 2LMN[14]). This dismisses unwanted effects that may arise from the applied periodic boundary conditions (PBC). The box was filled with single point charge (SPC) water molecules. Some water molecules were replaced by sodium and chloride ions to neutralize the system. The starting structures were subsequently energy-minimized with a steepest descent method for 3,000 steps. The results of these minimizations produced the starting structures for the MD simulations. The MD simulations were then carried out with a constant number of particles (N), pressure (P), and temperature (T) (NPT ensemble). The SETTLE algorithm[15] was used to constrain bond lengths and angles of the water molecules, while the LINCS algorithm[16] was used to constrain the bond lengths of the peptide. The long-range electrostatic interactions were calculated by the particle-mesh ewald (PME) method.[17] A constant pressure of 1 bar was applied with a coupling constant of 1.0 ps; peptide, water molecules, and ions were coupled separately to a bath at 300 K with a

coupling constant of 0.1 ps. The equation of motion was integrated at each 2 fs time steps. The tools available in GROMACS were utilized to analyze the MD trajectories. We used the most representative structures for the structural elucidation which were derived from the cluster analysis, where the trajectories are analyzed by grouping structurally similar frames [root-mean-square deviation (rmsd) cutoff of 0.30 nm], while the frame with the largest number of neighbors is denoted as a middle structure that represents that particular cluster. YASARA program[18] was used for visualization and preparation of the structural diagrams presented in this study.

Cell Viability Studies. Human neuroblastoma SK-N-BE(2)-M17 (M17) cells (ATCC, Manassa, VA, USA) were cultured in media containing 1:1 Minimum Essential Media (MEM; GIBCO, Grand Island, NY, USA), Ham's F12K Kaighn's Modification Media (F12K; GIBCO), 10% (v/v) fetal bovine serum (FBS; Atlanta Biologicals, Flowery Branch, GA, USA), 100 U/mL penicillin (GIBCO), and 100 mg/mL streptomycin (GIBCO). The cells were grown and maintained at 37 °C in a humidified atmosphere with 5% CO_2. M17 cells were seeded in a 96-well plate (150,000 cells in 100 μL per well) and treated with various concentrations of compounds (0–50 μM, 1% v/v DMSO) with and without $CuCl_2$ or $ZnCl_2$ (1:1 or 1:2 metal/ligand ratio) with and without $A\beta_{40}$ ($A\beta$:metal:compound = 10:10:20 μM). After 24 h incubation at 37 °C, 25 μL of MTT [3-(4,5-dimethylthiazol-2-yl)-2,5-diphenyltetrazolium bromide; 5 mg/mL in phosphate buffered saline (PBS), pH 7.4, GIBCO] was added to each well and the plates were incubated for 4 h at 37 °C. Formazan produced by the cells was dissolved in a solution containing *N,N*-dimethylformamide (DMF, 50% v/v aq) and sodium dodecyl sulfate (SDS, 20% w/v) overnight at room temperature. The absorbance at 600 nm was measured on a microplate reader.

S11

Trolox Equivalent Antioxidant Capacity (TEAC) Assay. The free organic radical scavenging capacity of compounds was determined by the TEAC assay in (a) EtOH or (b) M17 cell lysates. (a) The assay in EtOH was performed according to a previously reported method with slight modifications.[3a,3b] To generate blue ABTS cation radicals [ABTS$^{\bullet+}$; ABTS = 2,2'-azino-bis(3-ethylbenzothiazoline-6-sulfonic acid) diammonium salt; Sigma], ABTS (7.0 mM, Sigma) with potassium persulfate (2.5 mM) was dissolved in 5 mL of water and incubated for 16 h in the dark at room temperature. The resulting solution of ABTS$^{\bullet+}$ was diluted with EtOH to absorbance of *ca.* 0.7 at 734 nm. The solution of ABTS$^{\bullet+}$ (200 μL) was added to the wells of a clear 96 well plate and incubated at room temperature for 5 min in the plate reader. **L2-b1**, **L2-b2**, **PMA1**, **PMA2**, **DPA1**, **DPA2**, or Trolox (Trolox = 6-hydroxy-2,5,7,8-tetramethyl-chroman-2-carboxylic acid; dissolved in EtOH) [various concentrations: 0, 1, 2.5, 5, 7.5, 10, 15, and 20 μM] was incubated with the ABTS$^{\bullet+}$ solution at room temperature for 10 min. The percent inhibition was calculated according to the measured absorbance at 734 nm [% inhibition = $100 \times (A_0 - A)/A_0$] and plotted as a function of ligand concentration. The TEAC value of compounds was calculated as a ratio of the slope of the compound to that of Trolox. The measurements were carried out in triplicate. (b) The assay employing cell lysates was conducted following the protocol of the antioxidant assay kit purchased from Cayman Chemical Company (Ann Arbor, MI, USA) with minor modifications.[3a,3b] For the antioxidant assay using cell lysates, cells were seeded in a 6 well plate and grown to approximately 80-90% confluence. Cell lysates were prepared following a previously reported method with modifications.[19] M17 cells were washed once with cold PBS (pH 7.4, GIBCO) and harvested by gently pipetting off adherent cells with cold PBS. The cell pellet was generated by centrifugation (2,000 g for 10 min at 4 °C). This pellet was sonicated on ice (5 sec pulses, 3 times with 20 sec intervals between each pulse) in 2 mL of cold Assay Buffer

S12

(5 mM potassium phosphate, pH 7.4; 0.9% NaCl; 0.1% glucose). The cell lysates were centrifuged at 5,000 g for 10 min at 4 °C. The supernatant was removed and stored on ice until use. For standard and samples in 96 well plates, the supernatant of cell lysates (10 μL) was delivered followed by addition of compound, metmyoglobin, ABTS, and H_2O_2 in order. After 5 min incubation at room temperature on a shaker, absorbance values at 750 nm were recorded. The final concentrations (45, 90, 135, 180, 225, and 330 μM) of compounds and Trolox were used. The antioxidant concentration was calculated according to the measured absorbance [% inhibition = $100 \times (A_0 - A)/A_0$, where A_0 is absorbance of the supernatant of cell lysates]. The measurements were conducted in triplicate.

References

[1]   J.-S. Choi, J. J. Braymer, R. P. Nanga, A. Ramamoorthy, M. H. Lim, *Proc. Natl. Acad. Sci. USA* **2010**, *107*, 21990-21995.

[2]   J.-S. Choi, J. J. Braymer, S. K. Park, S. Mustafa, J. Chae, M. H. Lim, *Metallomics* **2011**, *3*, 284-291.

[3]   a) J. S. Derrick, R. A. Kerr, K. J. Korshavn, M. J. McLane, J. Kang, E. Nam, A. Ramamoorthy, B. T. Ruotolo, M. H. Lim, *Inorg. Chem.* **2016**, *55*, 5000-5013; b) S. Lee, X. Zheng, J. Krishnamoorthy, M. G. Savelieff, H. M. Park, J. R. Brender, J. H. Kim, J. S. Derrick, A. Kochi, H. J. Lee, C. Kim, A. Ramamoorthy, M. T. Bowers, M. H. Lim, *J. Am. Chem. Soc.* **2014**, *136*, 299-310; c) J. S. Derrick, R. A. Kerr, Y. Nam, S. B. Oh, H. J. Lee, K. G. Earnest, N. Suh, K. L. Peck, M. Ozbil, K. J. Korshavn, A. Ramamoorthy, R. Prabhakar, E. J. Merino, J. Shearer, J. Y. Lee, B. T. Ruotolo, M. H. Lim, *J. Am. Chem. Soc.* **2015**, *137*, 14785-14797.

[4]   a) A. Avdeef, S. Bendels, L. Di, B. Faller, M. Kansy, K. Sugano, Y. Yamauchi, *J. Pharm. Sci.* **2007**, *96*, 2893-2909; b) *BBB Protocol and Test Compounds*, *p*ION Inc., **2009**.

[5]   M. J. Frisch, G. W. Trucks, H. B. Schlegel, G. E. Scuseria, M. A. Robb, J. R. Cheeseman, G. Scalmani, V. Barone, B. Mennucci, G. A. Petersoon, *Gaussian 09, Revision A.02.*, Gaussian, Inc., **2009**.

[6]   R. Huang, S. Vivekanandan, J. R. Brender, Y. Abe, A. Naito, A. Ramamoorthy, *J. Mol. Biol.* **2012**, *416*, 108-120.

[7]   S. Vivekanandan, J. R. Brender, S. Y. Lee, A. Ramamoorthy, *Biochem. Biophys. Res. Commun.* **2011**, *411*, 312-316.

[8]   a) R. Soong, J. R. Brender, P. M. Macdonald, A. Ramamoorthy, *J. Am. Chem. Soc.* **2009**, *131*, 7079-7085; b) S. Narayanan, B. Reif, *Biochemistry* **2005**, *44*, 1444-1452.

[9]   C. Airoldi, E. Sironi, C. Dias, F. Marcelo, A. Martins, A. P. Rauter, F. Nicotra, J. Jimenez-Barbero, *Chem. Asian. J.* **2013**, *8*, 596-602.

[10]   M. W. Beck, S. B. Oh, R. A. Kerr, H. J. Lee, S. H. Kim, S. Kim, M. Jang, B. T. Ruotolo, J. Y. Lee, M. H. Lim, *Chem. Sci.* **2015**, *6*, 1879-1886.

[11]   O. Trott, A. J. Olson, *J. Comput. Chem.* **2010**, *31*, 455-461.

[12]   a) C. Oostenbrink, A. Villa, A. E. Mark, W.F. Van Gunsteren, *J. Comput. Chem.* **2004**, *25*, 1656-1676; b) E. Lindahl, B. Hess, *J. Mol. Model* **2001**, *7*, 306-317.

[13]   M. Coles, W. Bicknell, A. A. Watson, D. P. Fairlie, D. J. Craik, *Biochemistry* **1998**, *37*, 11064-11077.

[14]   A. T. Petkova, W. M. Yau, R. Tycko, *Biochemistry* **2006**, *45*, 498-512.

[15]   S. Miyamoto, P. A. Kollman, *J. Comput. Chem.* **1992**, *13*, 952-962.

[16]   B. Hess, H. Bekker, H. J. C. Berendsen, J. G. E. M. Fraaije, *J. Comput. Chem.* **1997**, *18*, 1463-1472.

[17]   D. M. York, T. A. Darden, L. G. Pedersen, *J. Chem. Phys.* **1993**, *99*, 8345-8348.

[18]   a) E. Krieger, G. Koraimann, G. Vriend, *Proteins* **2002**, *47*, 393-402; b) E. Krieger, G. Vriend, *Bioinformatics* **2002**, *18*, 315-318.

[19]   V. A. Spencer, J. M. Sun, L. Li, J. R. Davie, *Methods* **2003**, *31*, 67-75.

Table S1. Values (MW, $c$log$P$, HBA, HBD, PSA, logBB, and $-$logP_e)[a] for small molecules.

Calculation	L2-b1	L2-b2	PMA1	PMA2	DPA1	DPA2	Lipinski's rules and others
MW	227	270	108	151	199	285	≤ 450
$c$log$P$	2.31	2.47	-0.40	0.31	0.67	2.10	≤ 5.0
HBA	3	4	2	3	3	5	≤ 10
HBD	1	1	2	2	1	1	≤ 5
PSA	28.2	31.4	38.9	42.1	37.8	44.3	≤ 90
logBB	0.064	0.041	-0.507	-0.446	-0.327	-0.206	< -1.0 (poorly)
$-$logP_e	4.13 ± 0.01	4.52 ± 0.01	5.02 ± 0.06	4.68 ± 0.03	5.18 ± 0.05	4.47 ± 0.01	$-$log$P_e < 5.4$ (CNS+)
CNS$\pm$ prediction[b]	CNS+	CNS+	CNS+	CNS+	CNS+	CNS+	$-$log$P_e > 5.7$ (CNS$-$)

[a]MW, molecular weight; $c$log$P$, calculated logarithm of the octanol water partition coefficient; HBA, hydrogen bond acceptor atoms; HBD, hydrogen bond donor atoms; PSA, polar surface area; logBB = $-0.0148 \times$ PSA + $0.152 \times c$log$P$ + 0.139 (logBB < -1.0, poorly distributed to the brain); $-$logP_e values were determined using the Parallel Artificial Membrane Permeability Assay adapted for BBB (PAMPA-BBB) were then calculated by the PAMPA 9 Explorer software v. 3.8. [b]Prediction of a compound's ability to penetrate the central nervous system (CNS) on the basis of literature values. Compounds categorized as CNS+ have the possibility to penetrate the BBB and are available in the CNS.
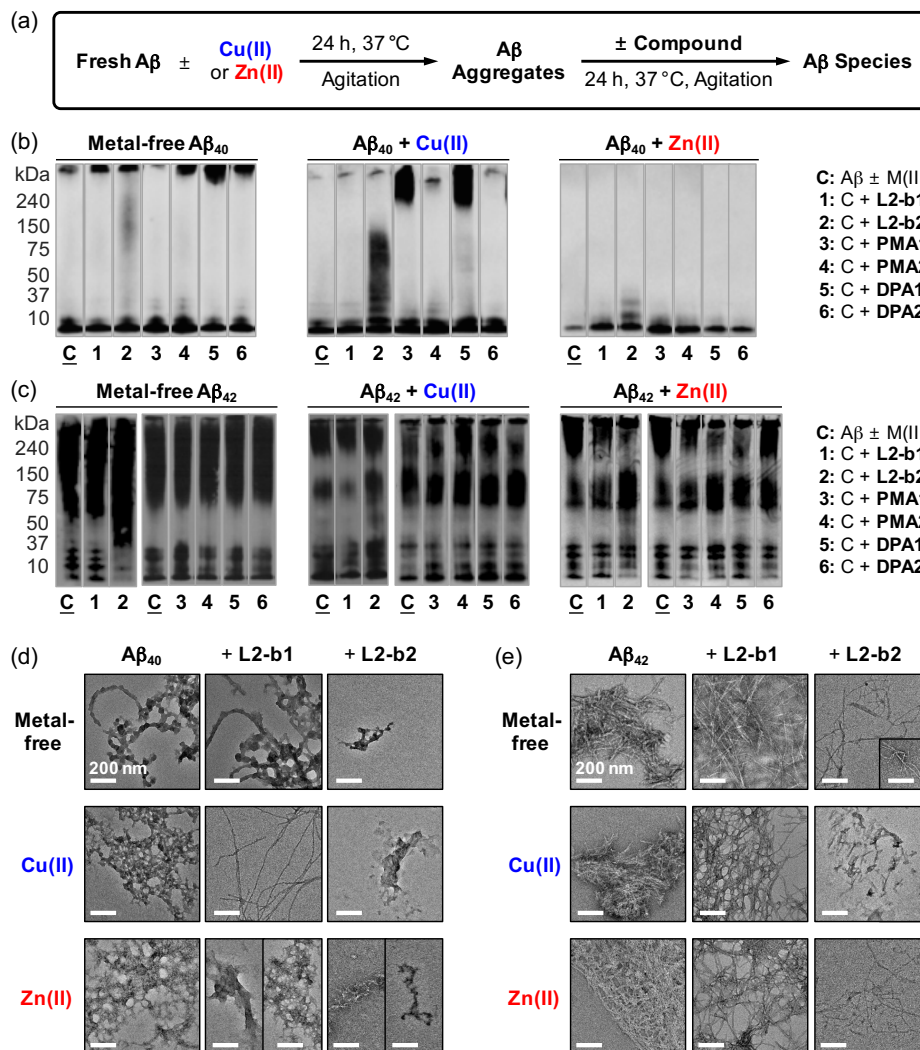
Figure S1. Influence of compounds on disassembly and further aggregation of metal-free Aβ and metal–Aβ aggregates. (a) Scheme of the disaggregation experiment. Analysis of size distributions of the resultant (b) $A\beta_{40}$ and (c) $A\beta_{42}$ by gel/Western blot with an anti-Aβ antibody (6E10). Conditions: $[A\beta] = 25$ μM; $[CuCl_2$ or $ZnCl_2] = 25$ μM; $[compound] = 50$ μM; pH 6.6 (for Cu(II) experiments) or pH 7.4 (for metal-free and Zn(II) experiments); 37 ˚C; constant agitation. TEM images of the resultant (d) $A\beta_{40}$ and (e) $A\beta_{42}$ aggregates from (b) and (c), respectively.
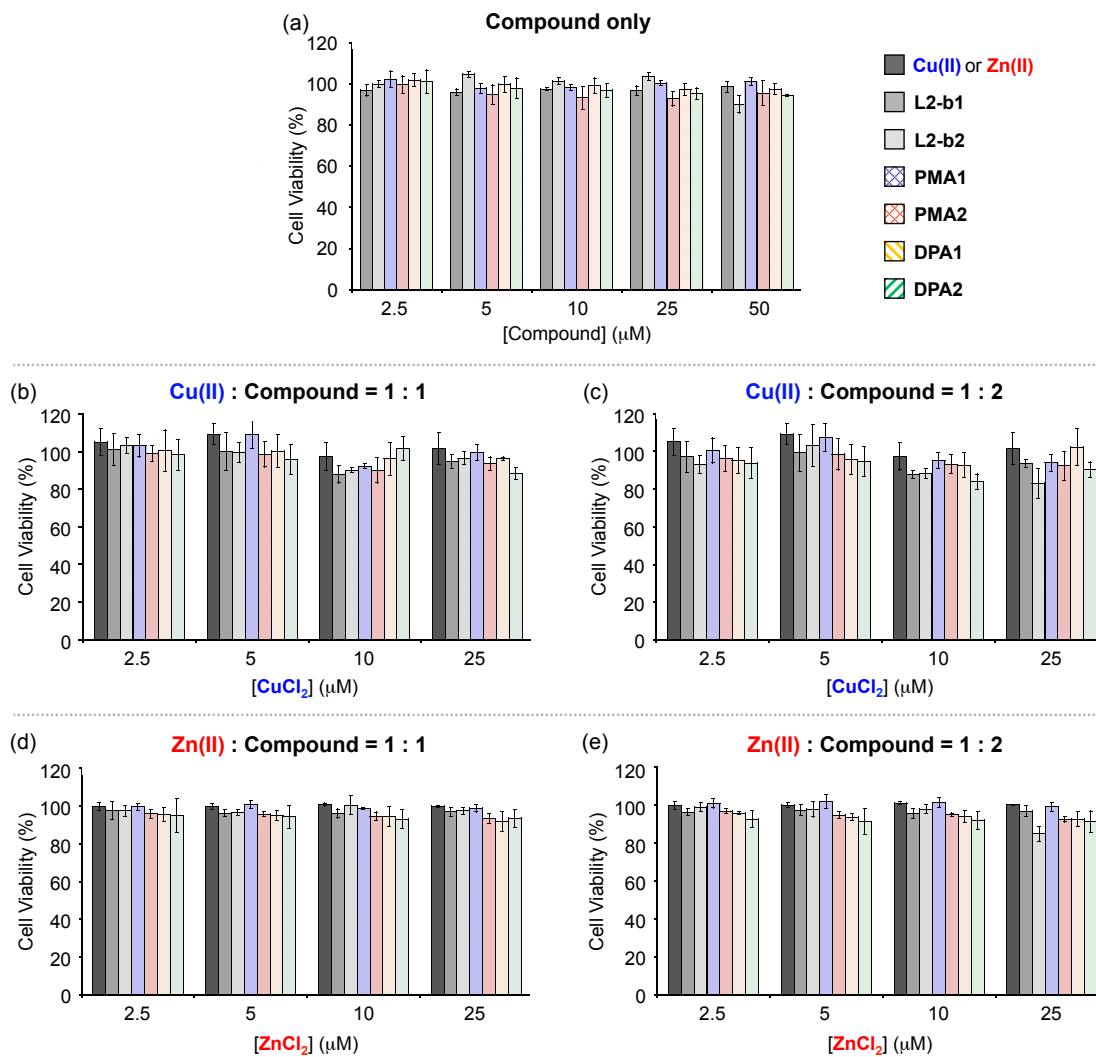
S17

Figure S2. Viability of cells treated with small molecules in both the absence and presence of CuCl$_2$ or ZnCl$_2$. M17 cells were treated with (a) various concentrations of compounds (2.5–50 μM; 1% v/v DMSO) with and without CuCl$_2$ [(b) 1:1 or (c) 1:2] or ZnCl$_2$ [(d) 1:1 or (e) 1:2]. Cell viability (%) was determined by the MTT assay compared to cells treated with DMSO only (0-1%, v/v). Error bars represent the standard error (SE) from three independent experiments.
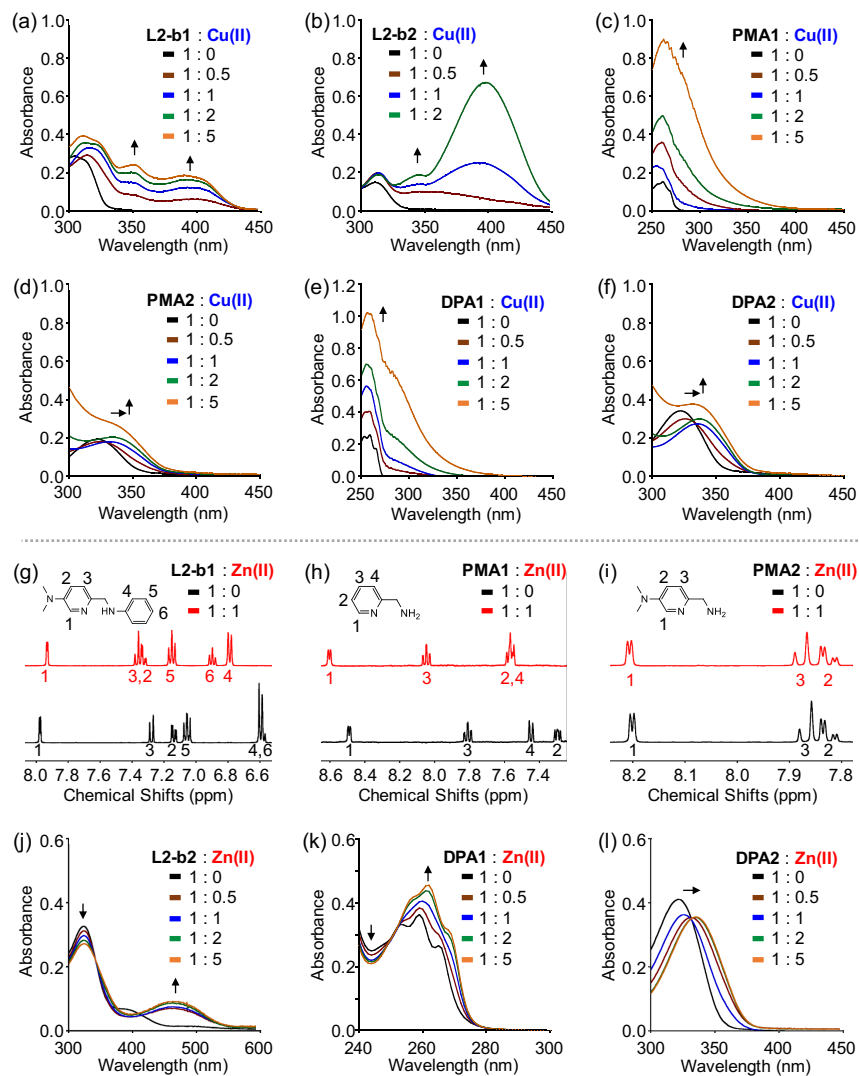
Figure S3. Metal binding studies of small molecules. UV−vis spectra of (a) **L2-b1**, (b) **L2-b2**, (c) **PMA1**, (d) **PMA2**, (e) **DPA1**, and (f) **DPA2** with CuCl$_2$ (up to 2 or 5 equiv) in EtOH. Conditions: [compound] = 25 μM (for **L2-b2**) or 50 μM (for **L2-b1**, **PMA1**, **PMA2**, **DPA1**, and **DPA2**); [CuCl$_2$] = 0–250 μM; room temperature; incubation for 30 min (for **L2-b1** and **L2-b2**) or 10 min (for **PMA1**, **PMA2**, **DPA1**, and **DPA2**). ^{1}H NMR spectra of (g) **L2-b1**, (h) **PMA1** (black) and (i) **PMA2** (black) with ZnCl$_2$ (1 equiv, red) in CD$_3$CN. Conditions: [**L2-b1**, **PMA1**, or **PMA2**] = 4 mM; [ZnCl$_2$] = 4 mM; room temperature; incubation for 5 min. UV−vis spectra of (j) **L2-b2**, (k) **DPA1**, and (l) **DPA2** with ZnCl$_2$ (up to 5 equiv) in EtOH. Conditions: [**L2-b2**, **DPA1**, and **DPA2**] = 50 μM; [ZnCl$_2$] = 0–250 μM; room temperature; incubation for 30 min (for **L2-b2**) or 10 min (for **DPA1** and **DPA2**).

S19

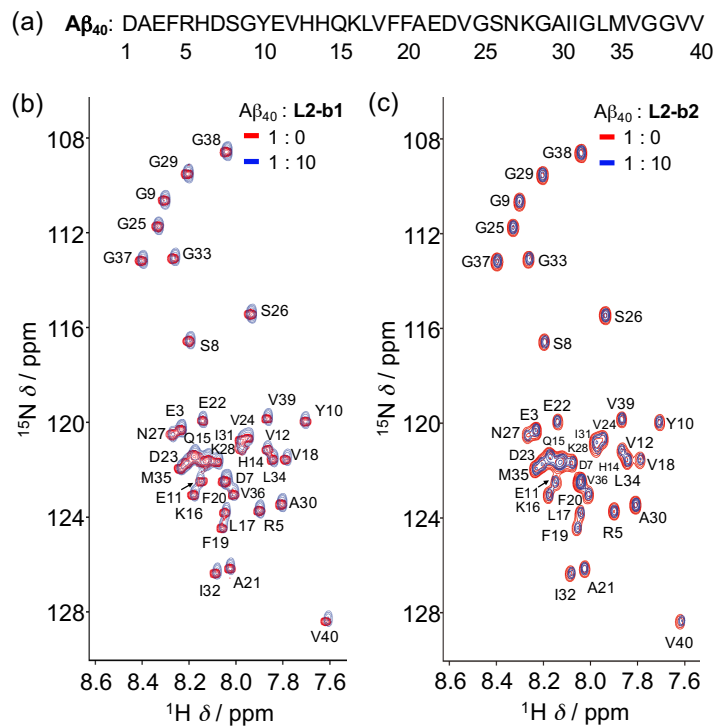**Figure S4.** Interactions of **L2-b1** or **L2-b2** with metal-free monomeric Aβ40. (a) Amino acid sequence of Aβ40. 2D ^{1}H–^{15}N SOFAST-HMQC NMR spectra of a solution of uniformly ^{15}N-labeled monomeric Aβ40 with (red) and without (blue) 10 mole % of (b) **L2-b1** or (c) **L2-b2**. Conditions: [Aβ40] = 80 μM; [**L2-b1** or **L2-b2**] = 0 or 800 μM; 20 mM PO4, pH 7.4, 50 mM NaCl; 7% D2O (v/v); 10 °C.

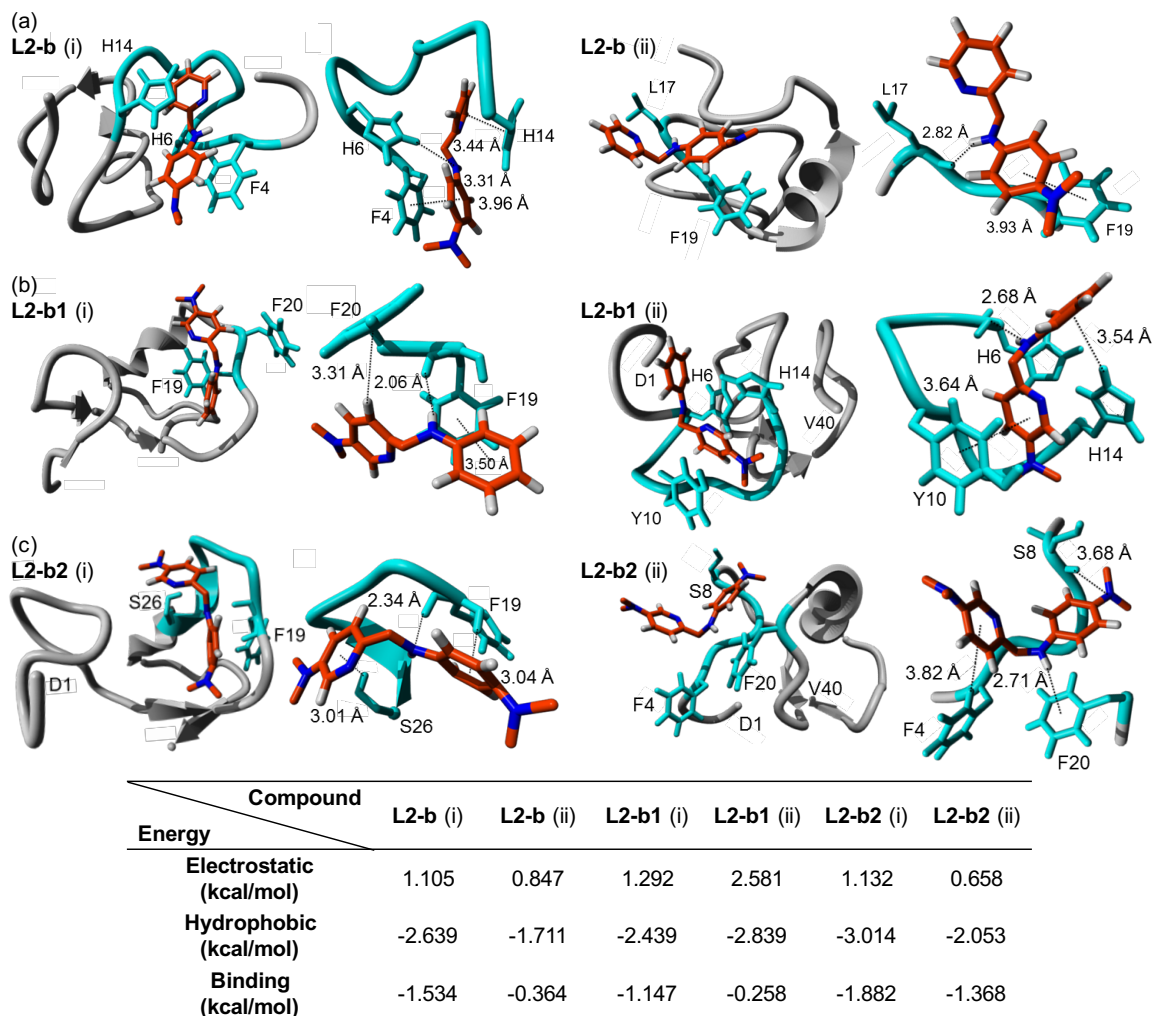| Compound / Energy	L2-b (i)	L2-b (ii)	L2-b1 (i)	L2-b1 (ii)	L2-b2 (i)	L2-b2 (ii)
Electrostatic (kcal/mol)	1.105	0.847	1.292	2.581	1.132	0.658
Hydrophobic (kcal/mol)	-2.639	-1.711	-2.439	-2.839	-3.014	-2.053
Binding (kcal/mol)	-1.534	-0.364	-1.147	-0.258	-1.882	-1.368

Figure S5. MD simulations showing interactions of **L2-b**, **L2-b1**, or **L2-b2** with monomeric Aβ$_{40}$. Possible sites and energy of interaction of Aβ$_{40}$ (PDB 1BA4) with (a) **L2-b**, (b) **L2-b1**, or (c) **L2-b2** after all-atom MD simulations are summarized. Right: The zoomed-in view of each binding site with residues showing interaction distances labeled in Å with dashed lines.
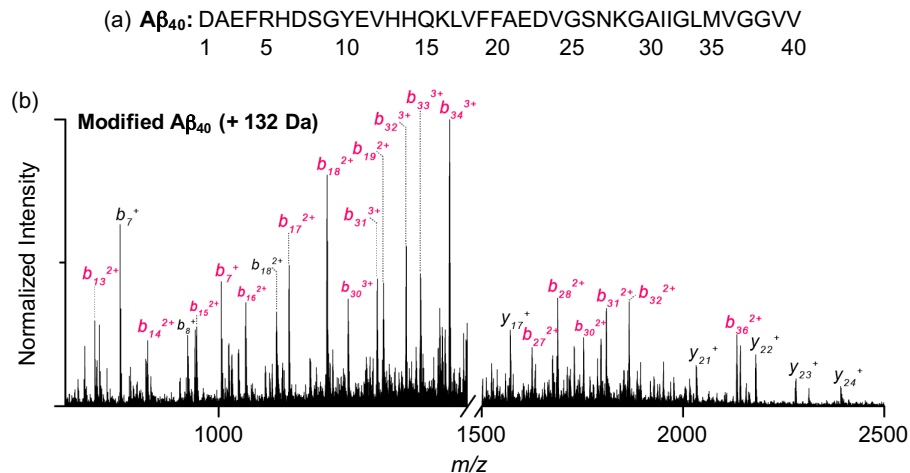
(a) **Aβ₄₀**: DAEFRHDSGYEVHHQKLVFFAEDVGSNKGAIIGLMVGGVV

Figure S6. Tandem mass spectrometry (MS/MS) sequencing studies of modified metal-free Aβ by **L2-b2**. (a) Amino acid sequence of Aβ₄₀. (b) The MS/MS study of the modified Aβ₄₀ generated upon treatment with **L2-b2**. These data support that the amino acid sequence of Aβ is directly interact with structurally transformed **L2-b2**. The Aβ species containing the identified +131.97 Da covalent modification are highlighted in magenta.
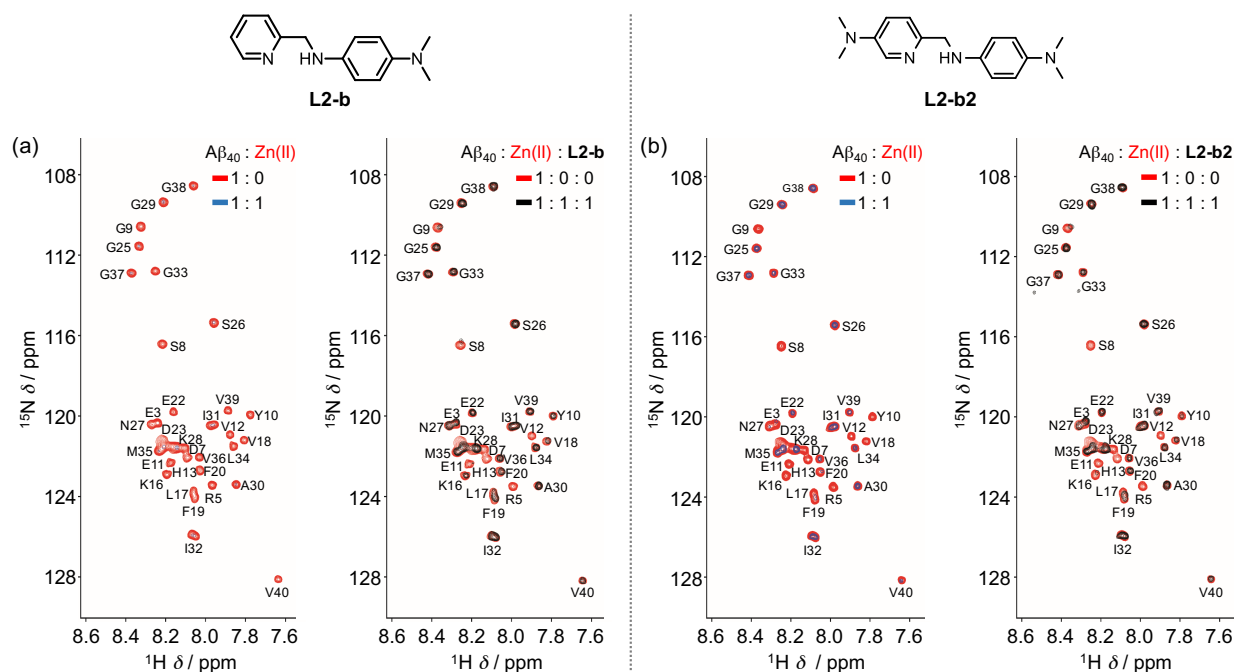
S22

Figure S7. Interactions of **L2-b** or **L2-b2** with Zn(II)-treated monomeric Aβ$_{40}$. 2D ^{1}H–^{15}N SOFAST-HMQC NMR spectra of a solution of uniformly ^{15}N-labeled monomeric Aβ$_{40}$ treated with Zn(II) (left) and (a) **L2-b** or (b) **L2-b2** (right). Conditions: [Aβ$_{40}$] = 80 μM; [ZnCl$_2$] = 80 μM; [**L2-b** or **L2-b2**] = 80 μM; 20 mM PO$_4$, pH 7.4, 50 mM NaCl; 7% v/v D$_2$O.
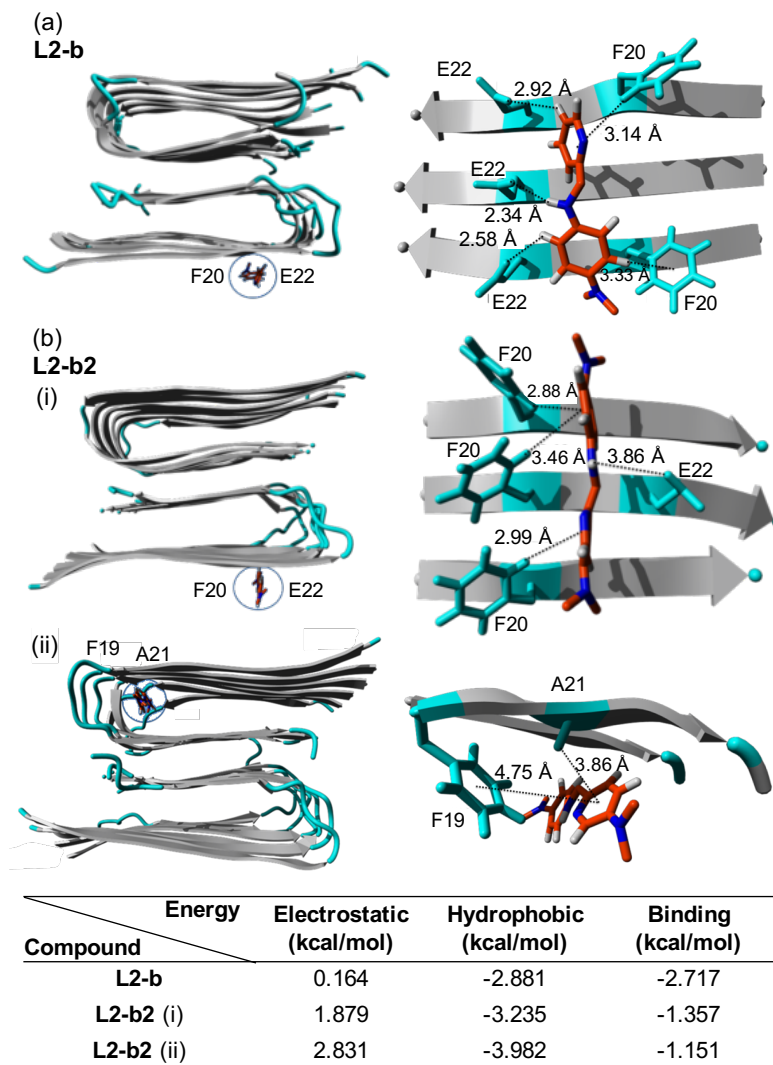
Figure S8. MD simulations showing interactions of **L2-b** or **L2-b2** with metal-free Aβ$_{40}$ fibrils. Potential binding sites and energy of interaction of (a) **L2-b** or (b) **L2-b2** with Aβ$_{40}$ fibrils (PDB 2LMN) after all-atom MD simulations are summarized. Right: The zoomed-in view of each binding site with residues showing interaction distances labeled in Å with dashed lines.

	Energy	Electrostatic (kcal/mol)	Hydrophobic (kcal/mol)	Binding (kcal/mol)
L2-b		0.164	-2.881	-2.717
L2-b2 (i)		1.879	-3.235	-1.357
L2-b2 (ii)		2.831	-3.982	-1.151